

Combined Crossed Molecular Beam and *ab Initio* Investigation of the Multichannel Reaction of Boron Monoxide (^{11}BO ; $X^2\Sigma^+$) with Propylene (CH_3CHCH_2 ; $X^1\text{A}'$): Competing Atomic Hydrogen and Methyl Loss Pathways

Surajit Maity, Beni B. Dangi, Dorian S. N. Parker, and Ralf I. Kaiser*

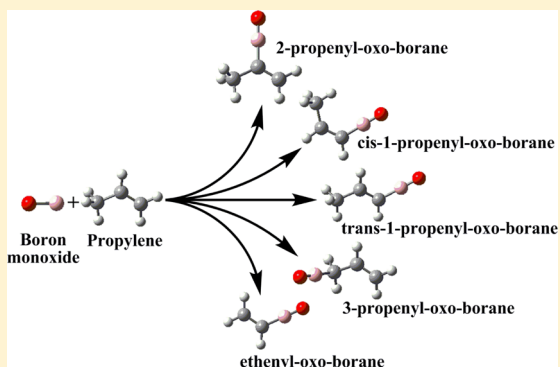
Department of Chemistry, University of Hawaii at Manoa, Honolulu, Hawaii 96822, United States

Yi An, Bing-Jian Sun, and A. H. H. Chang*

Department of Chemistry, National Dong Hwa University, Shoufeng, Hualien 974, Taiwan

S Supporting Information

ABSTRACT: The reaction dynamics of boron monoxide (^{11}BO ; $X^2\Sigma^+$) with propylene (CH_3CHCH_2 ; $X^1\text{A}'$) were investigated under single collision conditions at a collision energy of $22.5 \pm 1.3 \text{ kJ mol}^{-1}$. The crossed molecular beam investigation combined with *ab initio* electronic structure and statistical (RRKM) calculations reveals that the reaction follows indirect scattering dynamics and proceeds via the barrierless addition of boron monoxide radical with its radical center located at the boron atom. This addition takes place to either the terminal carbon atom (C1) and/or the central carbon atom (C2) of propylene reactant forming $^{11}\text{BOC}_3\text{H}_6$ intermediate(s). The long-lived $^{11}\text{BOC}_3\text{H}_6$ doublet intermediate(s) underwent unimolecular decomposition involving at least three competing reaction mechanisms via an atomic hydrogen loss from the vinyl group, an atomic hydrogen loss from the methyl group, and a methyl group elimination to form *cis-/trans-1-propenyl-oxo-borane* ($\text{CH}_3\text{CHCH}^{11}\text{BO}$), 3-propenyl-oxo-borane ($\text{CH}_2\text{CHCH}_2^{11}\text{BO}$), and ethenyl-oxo-borane ($\text{CH}_2\text{CH}^{11}\text{BO}$), respectively. Utilizing partially deuterated propylene (CD_3CHCH_2 and CH_3CDCD_2), we reveal that the loss of a vinyl hydrogen atom is the dominant hydrogen elimination pathway ($85 \pm 10\%$) forming *cis-/trans-1-propenyl-oxo-borane*, compared to the loss of a methyl hydrogen atom ($15 \pm 10\%$) leading to 3-propenyl-oxo-borane. The branching ratios for an atomic hydrogen loss from the vinyl group, an atomic hydrogen loss from the methyl group, and a methyl group loss are experimentally derived to be $26 \pm 8\%$: $5 \pm 3\%$: $69 \pm 15\%$, respectively; these data correlate nicely with the branching ratios calculated via RRKM theory of 19%:5%:75%, respectively.



1. INTRODUCTION

Reactions of the ground state boron monoxide (^{11}BO ; $X^2\Sigma^+$) radical with unsaturated hydrocarbons are of importance in understanding the formation of small boron–oxygen bearing hydrocarbons in boron combustion processes. Over recent decades, boron has been considered to be a promising candidate as a high energy propellant as it holds the highest energy density value by combustion of any element in the periodic table.^{1,2} However, a delayed and incomplete combustion of boron particles diminishes the energy release through the formation of an inert diboron trioxide (B_2O_3) layer over the unreacted boron. Boron is also considered as an additive in conventional carbon based jet fuel systems. The combustion of hydrocarbon based fuels can reach temperatures of up to 2000 K, high enough to remove the B_2O_3 layer. However, in these hydrogen and oxygen containing environments, the full energy release is still inaccessible due to the formation of HBO and HBO₂ intermediates.^{1,2} Extensive

investigations were performed both experimentally and theoretically over the past decades to understand the ignition and combustion processes of boron.^{2–9} Several gas phase kinetic models on the B/C/H/O (Yetter et al.)^{10,11} and B/C/H/O/F systems (Brown et al. and Zhou et al.)^{9,12} were developed aiming at a better gasification process of the B_2O_3 layer and an enhanced combustion process in hydrocarbon environments. Although the kinetic models developed by Zhou et al.⁹ and Brown et al.¹² are the most comprehensive, they lack crucial experimental input parameters such as the reaction products and their kinetics. Based on these models, Hussmann et al. developed a simplified gas phase kinetic model. However, they also emphasized requirements of accurate experimental parameters to execute the full chemical kinetics model.^{13,14}

Received: July 14, 2014

Revised: September 17, 2014

Published: September 19, 2014

Therefore, experimental and theoretical investigations of key bimolecular reactions in boron based combustion processes are necessary. Previously, our group systematically investigated the reaction dynamics of the formation of organo-boron species,¹⁵ utilizing the crossed molecular beam technique. These studies accessed the B/C/H system via the reaction of ground state boron atoms with key hydrocarbons such as acetylene,¹⁶ ethylene,¹⁷ methylacetylene,¹⁸ allene,¹⁹ dimethylacetylene,²⁰ and benzene.²¹

However, experimental parameters for the B/C/H/O system are still sparse; these data are crucial to develop complete boron combustion models. Note that the very first boron bearing species formed in the combustion of boron is the boron monoxide radical,^{12,22,23} which can react either with oxygen to form ultimately diboron trioxide (B_2O_3) or with the components of the hydrocarbon fuel to form B/C/H/O bearing molecules. For these reasons, our laboratory has started investigations of elementary reactions between boron monoxide and hydrocarbons such as acetylene (C_2H_2),²⁴ ethylene (C_2H_4),²⁵ methylacetylene (CH_3CCH),²⁶ dimethylacetylene (CH_3CCCH_3),²⁷ diacetylene ($HCCCCH$),²⁸ and benzene (C_6H_6)²⁹ using the crossed molecular beams technique.

In addition to the boron combustion chemistry, the boron monoxide radical ($BO; X^2\Sigma^+$) draws considerable interest from the physical organic community as it is isoelectronic with the cyano radical ($CN; X^2\Sigma^+$).^{30–32} Both boron monoxide and cyano radicals depict several similarities such as similar bond strengths (799 kJ mol⁻¹ vs 749 kJ mol⁻¹), ionization energies (13.3 eV vs 13.6 eV), and internuclear distances (1.205 Å vs 1.172 Å).²⁴ In both cases, the unpaired electron is preferentially located on the least electronegative atom, i.e., boron in BO and carbon in CN. A recent theoretical investigation on the vertical electron detachment energies of oxoboryl (-BO) substituted acetylene³³ revealed that the system is similar to the cyano substituted hydrocarbon systems. Therefore, the reactions of $BO(X^2\Sigma^+)$ and $CN(X^2\Sigma^+)$ with hydrocarbon molecules are expected to be similar with respect to the reaction mechanisms and products formed. Previously, the reactions of cyano radicals with hydrocarbons were explored experimentally and theoretically to understand the chemical reaction dynamics together with the thermodynamic properties (reaction exoergicity) of the products.^{34–39} Recent investigations of the reaction of boron monoxide radical with hydrocarbon molecules portrayed similarities and differences to the reactions of cyano radicals with hydrocarbons.^{24–27,40}

Further, the synthesis and characterizations of the organyloxo-borane (RBO) have attracted researchers due to the presence of strong boron–oxygen multiple bonds.^{41,42} Early studies of oxo-borane utilizing microwave and infrared spectrometry have revealed the evidence of a very strong boron–oxygen triple bond.^{43–45} However, oxo-boranes are very reactive due to the highly polar boron–oxygen bond and readily form oligomers to compensate for their intrinsic electron deficiency.^{46,47} The cyclo-oligomerization of RBO can be observed even at temperatures as low as 50 K,⁴⁶ and isolated oxo-boranes were reported either as reactive intermediates or in low temperature matrices.^{44,48,49} For example, methyl-oxo-borane (CH_3BO) and methylene-oxo-borane (CH_2BO) were identified in a low temperature argon matrix.⁴⁴ Recently, Braunschweig et al. synthesized a stable oxoboryl (BO) complex, ($Cy_3P_2Pt(BO)Br$ (Cy = cyclohexyl) for the first time.^{50,51} However, experimental evidence of stable

oxo-boranes are still sparse, and only limited theoretical investigations exist.^{52,53}

Here, the reaction of the boron monoxide ($^{11}BO; X^2\Sigma^+$) radical with propylene ($CH_3CHCH_2; X^1A'$) was investigated under single collision conditions utilizing the crossed molecular beam technique in an attempt to systematically elucidate the reaction dynamics of boron monoxide radical with unsaturated hydrocarbon molecules. We have also conducted the reaction with partially deuterated propylene ($CH_3CDCH_2; CD_3CHCH_2$) to ascertain the position of the atomic hydrogen loss. Finally, we compare the chemical reactivity of the boron monoxide radical with the isoelectronic reaction of CN radicals ($X^2\Sigma^+$) with CH_3CHCH_2 studied previously in our group under single collision conditions³⁷ along with the reaction.

2. EXPERIMENTAL AND DATA ANALYSIS

The reactions of the ground state boron monoxide radical ($BO; X^2\Sigma^+$) with propylene ($CH_3CHCH_2; X^1A'$) were conducted in a universal crossed molecular beams machine under single collision conditions.^{54–58} Briefly, a supersonic beam of ground state boron monoxide ($^{11}BO; X^2\Sigma^+$) was produced *in situ* via laser ablation of a boron rod at 266 nm and seeding the ablated boron in pure carbon dioxide carrier gas (CO_2 , 99.99%, BOC gases).⁵⁹ The fourth harmonic output of a Spectra-Physic Quanta-Ray Pro 270 Nd:YAG laser (266 nm) operating at a repetition rate of 30 Hz was focused with an output power of 15–20 mJ/pulse on the rotating boron rod using a lens with 1500 mm focal length. The carbon dioxide gas was released by a Proch-Trickl pulsed valve with a nozzle diameter of 1 mm operating at 60 Hz with 80 μ s pulse width and –350 V pulse amplitude.⁶⁰ A backing pressure of 4 atm was exploited, which yielded a pressure of 5×10^{-4} Torr inside the primary source chamber. The boron atoms likely reacted with the carbon dioxide to produce $^{11}BO(X^2\Sigma^+)$ via atomic oxygen abstraction; this radical beam was then passed through a skimmer of diameter 1 mm. A four-slot chopper wheel operating at a speed of 120 Hz was placed 18 mm downstream from the skimmer and selected a 11.2 μ s segment of the $^{11}BO(X^2\Sigma^+)$ beam with a peak velocity (v_p) of 1426 ± 35 ms⁻¹; the uncertainty refers to the averaged fluctuations of the peak velocities of the primary beam. Further, a speed ratio (S) of 2.2 ± 0.3 was obtained for the boron monoxide beam. The rovibrational levels of the boron monoxide radical were characterized *in situ* via laser-induced fluorescence (LIF) spectroscopy.⁶¹ Briefly, the $^2\Sigma^+$ electronic ground state of the boron monoxide radical was probed via the $A^2\Pi - X^2\Sigma^+$ transition. The (0,0) vibrational band near 425 nm was recorded by using the Nd:YAG pumped Lambda Physik Scanmate dye laser output of 10 μ J/pulse. The spectra were analyzed using the diatomic spectral simulation program developed by Tan.⁶² The rotational temperature was determined to be 250 K.⁶¹ This indicates that the ^{11}BO radicals have a maximum of 2 kJ mol⁻¹ of internal energy.^{25,61} The LIF spectrum of ^{11}BO radical did not show any (1,1) vibrational band; based on the signal-to-noise, less than 5% of ^{11}BO radical was suggested to reside in the $\nu = 1$ level.⁶¹

This segment of the primary beam was crossed by a second pulsed molecular beam of CH_3CHCH_2 perpendicularly in the interaction region. Propylene (Aldrich; 99%+) was released by a second Proch-Trickl pulsed valve operating at a repetition rate of 60 Hz with 80 μ s pulse width and backing pressure of 550 Torr characterized by a peak velocity of 840 ± 10 ms⁻¹ and speed ratio of $S = 11.0 \pm 0.2$. The peak collision energy between $^{11}BO(X^2\Sigma^+)$ and CH_3CHCH_2 was determined to be

$22.5 \pm 1.3 \text{ kJ mol}^{-1}$. Note that both pulsed valves, laser pulse, and the chopper wheel were synchronized by three digital pulse generators (Stanford Research System, DG535) with the help of two frequency dividers (Pulse Research Lab, PRL-220A). The time zero trigger originates from a photodiode, mounted on the top of the chopper wheel. The primary and the secondary pulsed valves were triggered 1882 and 1872 μs , respectively, after the time zero trigger pulse. The laser was triggered 156 μs after the trigger pulse of the primary pulsed valve.

The reactively scattered products were monitored using a triply differentially pumped quadrupole mass spectrometer (QMS) operated in the time-of-flight (TOF) mode, i.e., determining the flight time of an ion at a specific mass-to-charge ratio, after electron impact ionization of the neutral species by 80 eV electron energy with an emission current of 2 mA. The extracted ions pass through the quadrupole mass filter (Extrel QC 150) operated with an oscillator frequency of 2.1 MHz. Only ions with selected mass-to-charge ratio (m/z) can pass through the quadrupole mass filter and are accelerated toward a stainless steel target coated with a thin layer of aluminum maintained at a voltage of -22.5 kV. The ions hit the surface and initiate an electron cascade until it reaches an aluminum coated organic scintillator, whose photon cascade is detected by a photomultiplier tube (PMT, Burle, Model 8850) operated at -1.35 kV. The signal from the PMT was then filtered by a discriminator (Advanced Research Instruments, Model F-100TD; level, 1.6 mV) prior to feeding into a multichannel scaler (Stanford Research System SR430) to record the time-of-flight spectra.^{56,58} The detector is rotatable in the plane defined by the primary and the secondary reactant beams to allow recording angular resolved TOF spectra.

At each angle, up to 7.2×10^5 and 8.2×10^5 TOF spectra were accumulated for the atomic hydrogen and methyl loss channels, respectively, in batches of 51,200 TOF spectra. The recorded TOF spectra were then integrated and normalized to extract the product angular distribution in the laboratory frame. To gain information on the reaction dynamics, the experimental data were transformed into the center-of-mass (CM) reference frame utilizing a forward-convolution routine.^{63,64} This iterative method assumes an initial choice of angular flux distribution, $T(\theta)$, and the product translational energy distribution, $P(E_T)$, in the center-of-mass frame. Laboratory TOF spectra and the laboratory angular distribution were then calculated from the $T(\theta)$ and $P(E_T)$ functions and were averaged over a grid of Newton diagrams to account for the apparatus functions and the beam spreads in velocity and direction. Best fits were obtained by iteratively refining the adjustable parameters in the center-of-mass functions within the experimental error limits of, for instance, peak velocity, speed ratio, and error bars in the laboratory angular distribution. The product flux contour map, $I(\theta, u) = P(u) T(\theta)$, reports the intensity of the reactively scattered products (I) as a function of the CM scattering angle (θ) and product velocity (u). This plot is called the reactive differential cross-section and gives an image of the reaction. The branching ratios of the channels were calculated using the method proposed by Krajnovich et al.⁶⁵

3. THEORETICAL SECTION

Probable reaction paths in the reaction of $\text{BO}(X^2\Sigma^+)$ with $\text{CH}_3\text{CCCH}_3(X^1\text{A}_{1g})$, are explored by *ab initio* electronic structure calculations. The intermediates, transition states,

and dissociation products are characterized such that their optimized geometries and harmonic frequencies are obtained at the level of the hybrid density functional theory, the unrestricted B3LYP/cc-pVTZ.^{66,67} The energies are refined with the coupled cluster^{68–71} CCSD(T)/cc-pVTZ with B3LYP/cc-pVTZ zero-point energy corrections. The electronic structure calculations were performed using the GAUSSIAN-03 program.⁷² Further, assuming the energy is equilibrated among the molecular degrees of freedom before the reaction occurs, and provided the energy is conserved such as in molecular beam experiments, the rate constants for the individual steps

were predicted via RRKM theory. For a reaction $A^* \xrightarrow{k} A^\ddagger \rightarrow P$, where A^* is the energized reactant, A^\ddagger represents the transition state, and P are the products, the rate constant $k(E)$ may be expressed as

$$k(E) = \frac{\sigma}{h} \frac{W^\ddagger(E - E^\ddagger)}{\rho(E)} \quad (1)$$

where σ is the symmetry factor, W^\ddagger the number of states of the transition state, E^\ddagger the transition state energy, and ρ the density of states of the reactant. ρ and W^\ddagger are computed by saddle-point method, and molecules are treated as collections of harmonic oscillators whose harmonic frequencies are obtained by B3LYP/cc-pVTZ as described previously.⁷³ These rate constants were also exploited to predict the branching ratios of the reaction.⁷³

4. RESULTS

4.1. Laboratory Data. In the $^{11}\text{BO}(X^2\Sigma^+; 27 \text{ amu})-\text{CH}_3\text{CHCH}_2(X^1\text{A}'; 42 \text{ amu})$ system, we recorded reactive scattering signal at mass-to-charge ratios $m/z = 68 \text{ amu}$ ($^{11}\text{BOC}_3\text{H}_5^+$) (Figure 1) and $m/z = 67 \text{ amu}$

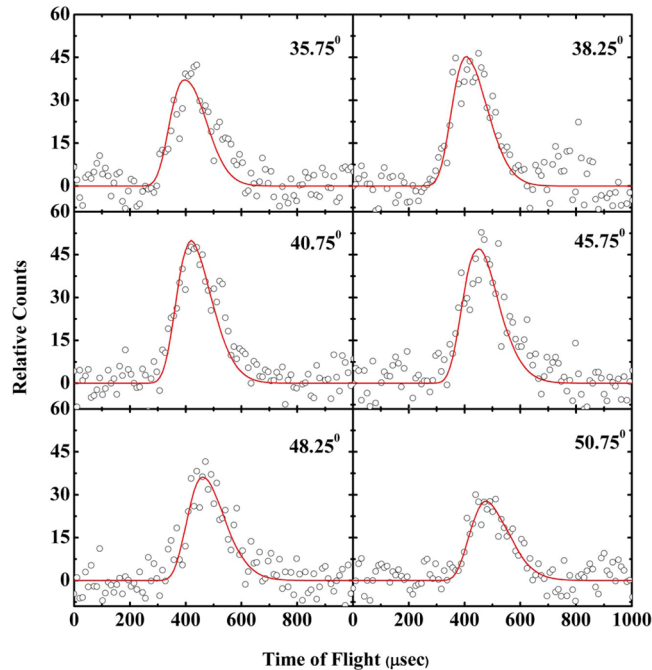


Figure 1. Time-of-flight spectra recorded at $m/z = 68 \text{ amu}$ ($^{11}\text{BOC}_3\text{H}_5^+$) at various angles for the reaction between $^{11}\text{BO}(X^2\Sigma^+)$ with $\text{CH}_3\text{CHCH}_2(X^1\text{A}')$ at a collision energy of $22.5 \pm 1.3 \text{ kJ mol}^{-1}$. The circles indicate the experimental data, and the solid lines indicate the calculated fit.

($^{11}\text{BOC}_3\text{H}_4^+ / ^{10}\text{BOC}_3\text{H}_5^+$) for the atomic hydrogen and/or molecular hydrogen loss pathways, respectively. Further, TOF spectra were recorded at $m/z = 54$ amu ($^{11}\text{BOC}_2\text{H}_3^+$; Figure 2) to probe the methyl group (CH_3) loss channel. After scaling, the TOF spectra recorded at $m/z = 68$ amu and $m/z = 67$ amu depicted identical profiles.

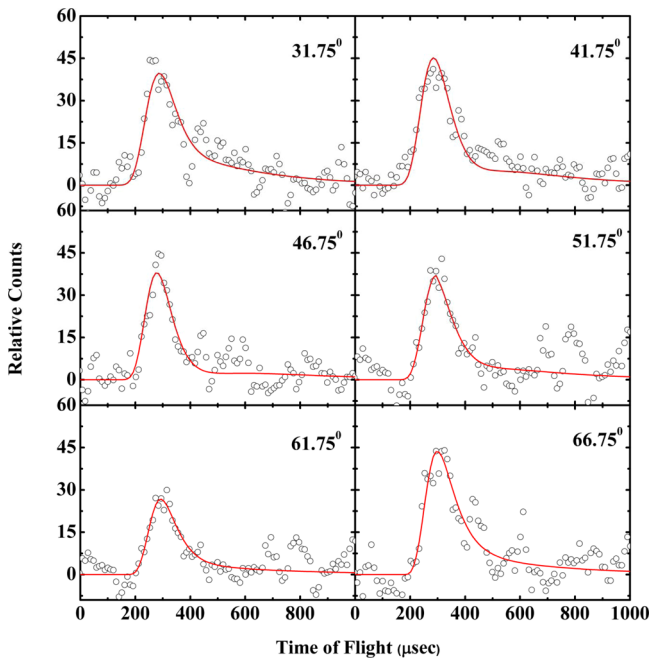


Figure 2. Time-of-flight spectra recorded at $m/z = 54$ amu ($^{11}\text{BOC}_2\text{H}_3^+$) at various angles for the reaction between $^{11}\text{BO}(X^2\Sigma^+)$ with $\text{CH}_3\text{CHCH}_2(X^1\text{A}')$ at a collision energy of $22.5 \pm 1.3 \text{ kJ mol}^{-1}$. The circles indicate the experimental data, and the solid lines indicate the calculated fit.

These observations indicate that the ions at $m/z = 67$ amu originate from dissociative ionization of the $^{11}\text{BOC}_3\text{H}_5$ product (68 amu) in the electron impact ionizer of the detector. Therefore, in the reaction of $^{11}\text{BO}(X^2\Sigma^+)$ with $\text{CH}_3\text{CHCH}_2(X^1\text{A}')$, the atomic hydrogen loss channel leading to the formation of $^{11}\text{BOC}_3\text{H}_5$ isomer(s) is confirmed via the observation of the reactive scattering signal observed at $m/z = 68$ amu ($^{11}\text{BOC}_3\text{H}_5$), and the molecular hydrogen loss channel is closed. In addition, the TOF spectra recorded at $m/z = 54$ amu ($^{11}\text{BOC}_2\text{H}_3^+$) (methyl group loss) show distinctly different profiles from those TOF spectra obtained at $m/z = 68$ amu (atomic hydrogen loss; $^{11}\text{BOC}_3\text{H}_5^+$). Therefore, we can conclude from the raw data that the TOF spectra recorded at $m/z = 54$ amu do not originate from the dissociative ionization of the $^{11}\text{BOC}_3\text{H}_5$ parent in the electron impact ionizer, but likely from the methyl loss channel. For both the atomic hydrogen ($m/z = 68$ amu) and methyl group loss channels ($m/z = 54$ amu), the laboratory angular distributions were obtained by integrating the TOF spectra taken for the product $^{11}\text{BOC}_3\text{H}_5$ at $m/z = 68$ amu (Figure 3) and $^{11}\text{BOC}_2\text{H}_3$ at $m/z = 54$ amu (Figure 4), respectively.

In the case of the atomic hydrogen loss, the TOF spectra (Figure 1) and laboratory angular distribution (Figure 3) were fit with a single channel and a product mass combination of 68 amu ($^{11}\text{BOC}_3\text{H}_5$) plus 1 amu (H). Here, the angular distribution extends at least 40.0° in the scattering plane defined by the primary and secondary molecular beams. The

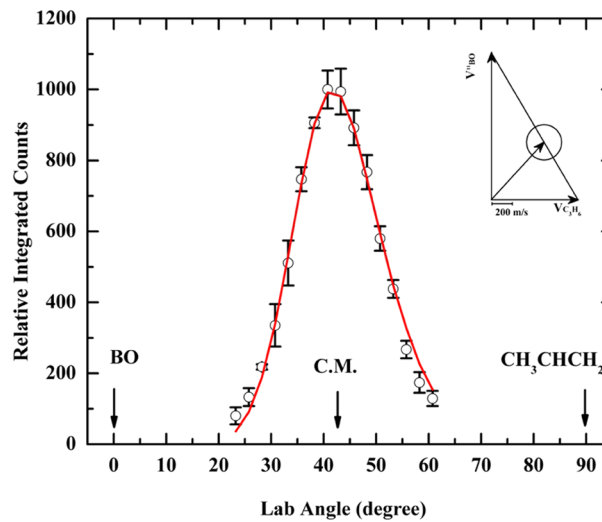


Figure 3. Laboratory angular distribution of $^{11}\text{BOC}_3\text{H}_5^+$ ions ($m/z = 68$ amu) recorded for the reaction of $^{11}\text{BO}(X^2\Sigma^+)$ with $\text{CH}_3\text{CHCH}_2(X^1\text{A}')$ at a collision energy of $22.5 \pm 1.3 \text{ kJ mol}^{-1}$. The circles and error bars indicate the experimental data, and the solid line indicates the calculated distribution. The inset shows the Newton diagram of the atomic hydrogen loss reaction at a collision energy of $22.5 \pm 1.3 \text{ kJ mol}^{-1}$.

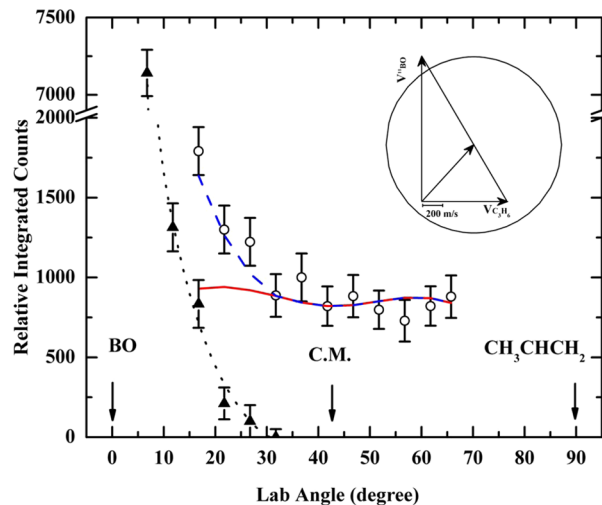


Figure 4. Laboratory angular distribution of $^{11}\text{BOC}_2\text{H}_3^+$ ions ($m/z = 54$ amu) recorded for the reaction of $^{11}\text{BO}(X^2\Sigma^+)$ with $\text{CH}_3\text{CHCH}_2(X^1\text{A}')$ at a collision energy of $22.5 \pm 1.3 \text{ kJ mol}^{-1}$. The open circles represent the experimental data, and the solid line (red) indicates the calculated distribution with the best fit center-of-mass functions. The solid triangles represent an inelastic scattering signal recorded at $m/z = 54$ amu ($^{10}\text{B}^{11}\text{B}_4^+$ and/or $^{11}\text{B}_2\text{O}_2^+$) in a test reaction of boron monoxide with Ar under identical experimental conditions, and the dotted line indicates the numerical fit of the inelastic scattering data. The dashed line (blue) indicates the sum of the calculated distribution (solid line) and the numerical fit (dotted line). The inset shows the Newton diagram of the methyl loss reaction at a collision energy of $22.5 \pm 1.3 \text{ kJ mol}^{-1}$.

angular distribution peaks at $41.5 \pm 1.0^\circ$ close to the CM angle of $42.6 \pm 1.0^\circ$. The nearly symmetric laboratory angular distribution around the center-of-mass angle suggests that the reaction proceeds via indirect (complex forming) scattering dynamics involving $^{11}\text{BOC}_3\text{H}_6$ reaction intermediate(s). Considering the methyl loss channel, both the TOF (Figure 2) and laboratory angular distribution (Figure 4) were also fit

with a single channel and a product mass combination of 54 amu ($^{11}\text{BOC}_2\text{H}_3$) and 15 amu (CH_3). As expected from the significantly enhanced scattering range due to the product mass combination of 54 and 15 amu and the reaction exoergicity, the laboratory angular distribution is very broad. Therefore, the products are scattered over a wide angular range, i.e., of about 160° based on the Newton diagram. It should be mentioned that at angles closer to the primary beam, we found evidence of interference at $m/z = 54$ amu from the nonreactively scattered $^{10}\text{B}^{11}\text{B}_4$ and/or $^{11}\text{B}_2\text{O}_2$ species produced in the primary beam. However, the nonreactively scattered signals at $m/z = 54$ amu diminished rapidly once we moved away from the primary beam toward the center-of-mass angle at $42.6 \pm 1.0^\circ$. A test reaction between the ^{11}BO beam with argon (Ar) clearly supports the preceding statement.

Having identified two distinct exit channels, i.e., the atomic hydrogen and methyl loss pathways, we are now focusing our attention on the position of the atomic hydrogen loss. In the propylene reactant, the hydrogen atoms can be released either from the vinyl group or from the methyl group. Therefore, we utilized partially deuterated reactants propylene- $3,3,3-d_3$ ($\text{CD}_3\text{CHCH}_2; X^1\text{A}'$) and propylene- $1,1,2-d_3$ ($\text{CH}_3\text{CDCD}_2; X^1\text{A}'$) to elucidate the position of the atomic hydrogen loss. In both cases, the atomic hydrogen loss products of general molecular formula $^{11}\text{BOC}_3\text{D}_3\text{H}_2$ can only be detected at $m/z = 71$ amu; the center-of-mass TOF spectra are depicted in Figure 5. These findings clearly confirm the existence of at least two

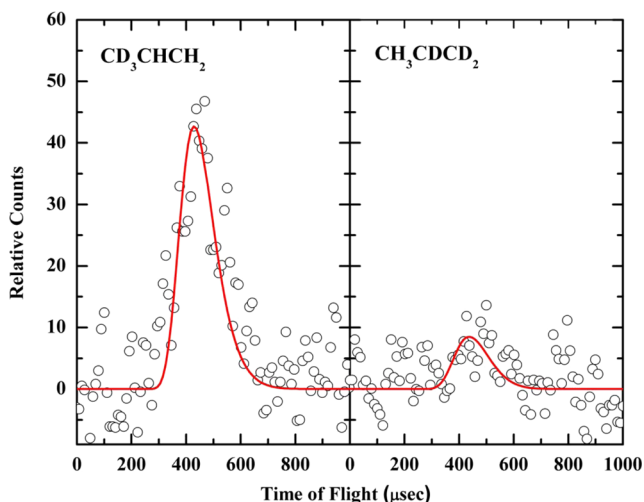


Figure 5. Time-of-flight data at the center-of-mass angles recorded for the atomic hydrogen loss pathway in the reaction of $^{11}\text{BO}(X^2\Sigma^+)$ with $\text{CD}_3\text{CHCH}_2(X^1\text{A}')$ (left) and $\text{CH}_3\text{CDCD}_2(X^1\text{A}')$ (right) at $m/z = 71$ amu ($^{11}\text{BOC}_3\text{D}_3\text{H}_2^+$).

distinct atomic hydrogen loss channels, from the vinyl group and from the methyl group of propylene. An integration of these TOF spectra indicates that the atomic hydrogen loss from the vinyl group presents the major product channel ($85 \pm 10\%$) compared to the atomic hydrogen loss from the methyl group ($15 \pm 10\%$) of propylene molecule. In the CD_3CHCH_2 and CH_3CDCD_2 systems, the deuterium elimination products ($^{11}\text{BOC}_3\text{D}_2\text{H}_3$) would have masses of 70 amu. Therefore, deuterium loss channels do not contribute to the signal at $m/z = 71$ amu. Note that for both partially deuterated propylene systems, we recorded the TOF spectra only at the center-of-

mass angle due to the low signal counts and the high costs of the partially deuterated chemicals.

4.2. Center-of-Mass System. To elucidate the reaction dynamics of the boron monoxide–propylene system, the laboratory data were transformed into the center-of-mass reference frame utilizing a forward convolution routine as described in Experimental and Data Analysis. The corresponding center-of-mass angular distribution and the translational energy distribution are shown in Figures 6 and 7 for the atomic

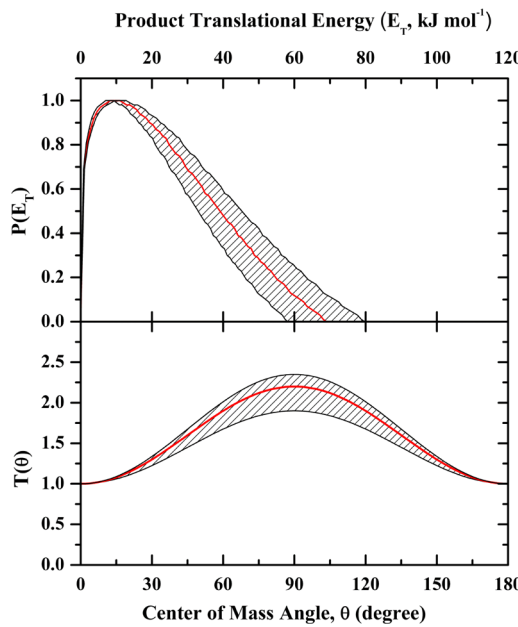


Figure 6. Center-of-mass translational energy distribution (top) and center-of-mass angular distribution (bottom) for the atomic hydrogen loss pathway leading to $^{11}\text{BOC}_3\text{H}_5$ isomers in the reaction between $^{11}\text{BO}(X^2\Sigma^+)$ with $\text{CH}_3\text{CHCH}_2(X^1\text{A}')$. The hatched areas indicate the acceptable lower and upper limits of the fits, and the solid red line defines the best fit functions.

hydrogen loss and methyl group loss pathways, respectively. First we focus on the atomic hydrogen loss. Figure 6 (top) presents the center-of-mass translational energy distribution, $P(E_T)$, obtained for the $^{11}\text{BOC}_3\text{H}_5$ plus atomic hydrogen channel; this distribution depicts a maximum translational energy release, E_{\max} of $68 \pm 11 \text{ kJ mol}^{-1}$. From the conservation of energy, we can calculate the reaction exoergicity by subtracting the collision energy ($22.5 \pm 1.3 \text{ kJ mol}^{-1}$) from the maximum translational energy ($68 \pm 11 \text{ kJ mol}^{-1}$) for those molecules born without internal excitation. This leads to a reaction exoergicity of $46 \pm 12 \text{ kJ mol}^{-1}$ to form $^{11}\text{BOC}_3\text{H}_5$ isomer(s) plus atomic hydrogen. It is worth mentioning that LIF study shows ^{11}BO is efficiently cooled by the supersonic expansion and only has a maximum of 2.0 kJ mol^{-1} of internal energy. If we consider that propylene is also efficiently cooled by the supersonic expansion, we can subtract the maximum internal energy from the reaction exoergicity to obtain a value of the reaction exoergicity of $44 \pm 12 \text{ kJ mol}^{-1}$. Further, the best fit center-of-mass translational energy distribution, $P(E_T)$, shows that the maximum of the flux distribution is located away from zero translational energy at about $8-14 \text{ kJ mol}^{-1}$. This suggests the presence of an exit barrier and hence a tight exit transition state (repulsive bond rupture with a significant electron rearrangement) from the decomposing complex to the

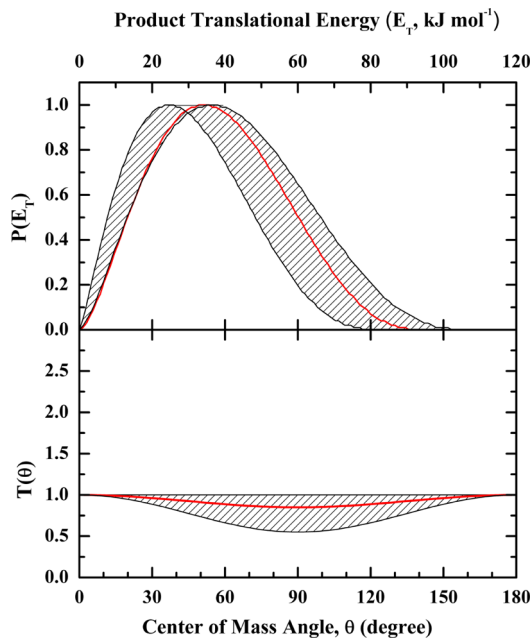


Figure 7. Center-of-mass translational energy distribution (top) and center-of-mass angular distribution (bottom) for the methyl loss pathway leading to $^{11}\text{BOC}_2\text{H}_3$ isomer(s) in the reaction between $^{11}\text{BO}(X^2\Sigma^+)$ with $\text{CH}_3\text{CHCH}_2(X^1\text{A}')$. The hatched areas indicate the acceptable lower and upper limits of the fits, and the solid red line defines the best fit functions.

products.⁷⁴ Finally, the center-of-mass translational energy distribution allows us to determine the average amount of energy released into the translational degrees of freedom of the products, i.e., $34 \pm 6\%$ of the total available energy.

In the case of the methyl loss channel (Figure 7; top), the center-of-mass translational energy distribution depicts a maximum translational energy (E_{\max}) release of $93 \pm 18 \text{ kJ mol}^{-1}$. The exoergicity of the $^{11}\text{BOC}_2\text{H}_3$ plus CH_3 reaction is determined to be $71 \pm 19 \text{ kJ mol}^{-1}$, by subtracting the collision energy ($22.5 \pm 1.3 \text{ kJ mol}^{-1}$) from the E_{\max} . Further, the reaction exoergicity can be corrected to $69 \pm 19 \text{ kJ mol}^{-1}$ by subtracting the maximum internal energy (2.0 kJ mol^{-1}) of ^{11}BO radicals. Additionally, the distribution peaks away from

zero translational energy at about $25\text{--}40 \text{ kJ mol}^{-1}$. This observation also indicates the presence of a tight exit transition state while $^{11}\text{BOC}_3\text{H}_6$ intermediate decomposes to the products: $^{11}\text{BOC}_2\text{H}_3$ and CH_3 . Finally, the fraction of available energy channelling into the translational degrees of freedom of the products is calculated to be $42 \pm 10\%$.

The center-of-mass angular distributions, $T(\theta)$ s, deliver additional information on the chemical dynamics of the title reaction; they are depicted in Figure 6 (bottom) and Figure 7 (bottom) for the atomic hydrogen and methyl loss pathways, respectively. Both distributions show intensities over the whole angular range from 0° to 180° . These findings are indicative of indirect scattering dynamics involving the formation of $^{11}\text{BOC}_3\text{H}_6$ collision complexes for both atomic hydrogen and methyl loss pathways.⁷⁵ Further, both distributions are forward–backward symmetric with respect to 90° . This forward–backward symmetry proposes that the lifetime of the decomposing $^{11}\text{BOC}_3\text{H}_6$ complexes, which emit the hydrogen atom and the methyl group, is longer than their rotation periods.⁷⁵ However, the best fit $T(\theta)$ distributions for both the atomic hydrogen and the methyl loss channels hold a striking difference. In the case of atomic hydrogen loss channel, the best fit $T(\theta)$ depicts a distribution maximum at 90° , whereas the best fit $T(\theta)$ for the methyl loss channel depicts a minimum at 90° . These findings infer geometrical constraints in the exit channels.⁷⁵ Considering the atomic hydrogen loss channel, the hydrogen atom is suggested to be emitted almost perpendicularly to the plane of the decomposing $^{11}\text{BOC}_3\text{H}_6$ complex, i.e., nearly parallel to the total angular momentum vector. However, in the case of the methyl loss channel, the elimination of the methyl group occurs preferentially within the plane of the fragmenting $^{11}\text{BOC}_3\text{H}_6$ complex, i.e., almost perpendicularly to the total angular momentum vector.⁷⁵ These findings are also compiled in the flux contour map (Figure 8). The branching ratios for atomic hydrogen loss from the vinyl group, atomic hydrogen loss from the methyl group, and the methyl loss pathways are calculated to be $26 \pm 8\%:5 \pm 3\%:69 \pm 15\%$, respectively.

5. THEORETICAL RESULTS

The reaction of the $\text{BO}(X^2\Sigma^+)$ radical with $\text{CH}_3\text{CHCH}_2(X^1\text{A}')$ was investigated computationally. The computations (Figures 9

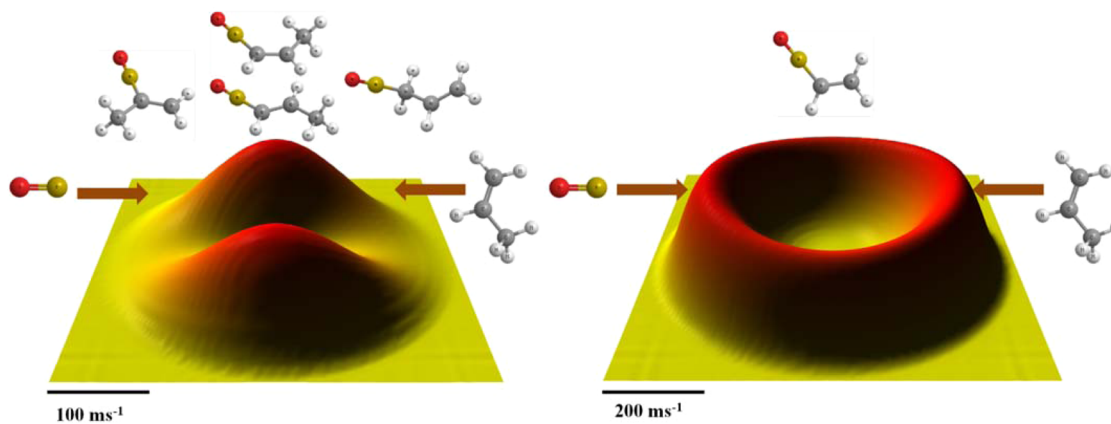


Figure 8. Flux contour maps of the competitive atomic hydrogen (left) and methyl loss (right) pathways in the crossed beam reaction of boron monoxide radicals with propylene leading to the formation of *cis*-/*trans*-1-propenyl-oxo-borane ($\text{CH}_3\text{CHCH}^{11}\text{BO}$), 2-propenyl-oxo-borane ($\text{CH}_3\text{C}^{(11)}\text{BOCH}_2$), and 3-propenyl-oxo-borane ($\text{CH}_2\text{CHCH}_2^{11}\text{BO}$) (hydrogen loss channel) and ethenyl-oxo-borane ($\text{CH}_2\text{CH}^{11}\text{BO}$) (methyl loss channel).

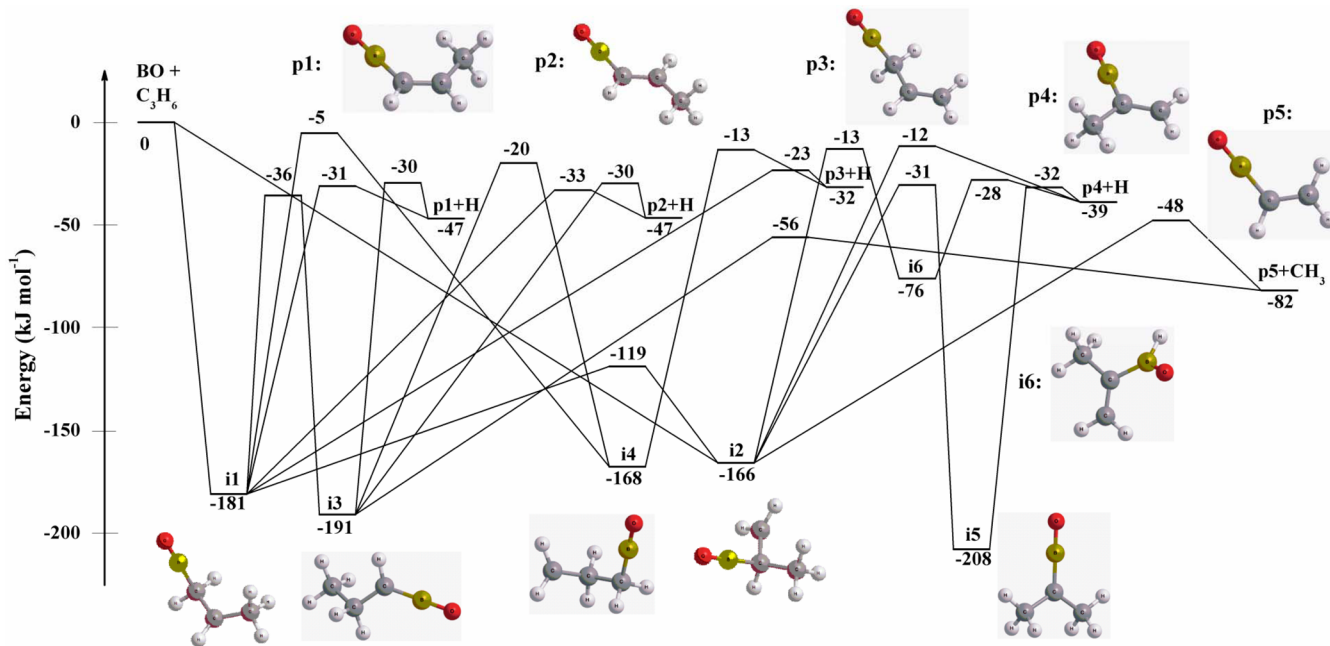


Figure 9. Schematic representation of the computed $^{11}\text{BOC}_3\text{H}_6$ potential energy surface (PES).

and 10) predict the existence of six BOC_3H_6 intermediates (**i1–i6**) which subsequently lead to five potential product channels (**p1–p5**) involving atomic hydrogen loss (**p1–p4**) and methyl group elimination (**p5**). In detail, the reaction between boron monoxide and propylene was found to proceed via the barrierless addition of the boron monoxide radical with its radical center located on the boron atom to either the terminal carbon atom (C1) and/or the central carbon atom (C2) of CH_3CHCH_2 reactant forming BOC_3H_6 intermediates **i1** (-181 kJ mol^{-1}) and **i2** (-166 kJ mol^{-1}). Intermediate **i1** can undergo three competing unimolecular decomposition pathways via atomic hydrogen loss from C1 and C3 carbon atoms of the propylene moiety. The atomic hydrogen elimination from the C1 carbon atom can lead to the formation of cis (**p1**) and trans (**p2**) isomers of $\text{CH}_3\text{CHCH}^{11}\text{BO}$ with overall reaction exoergicities of 47 kJ mol^{-1} . The atomic hydrogen elimination from the methyl group of **i1** can lead to the formation of $\text{CH}_2\text{CHCH}^{11}\text{BO}$ (**p3**) in an overall exoergic reaction (-32 kJ mol^{-1}). The reactions leading to **p1**, **p2**, and **p3** proceed via tight exit transition states residing 14, 16, and 9 kJ mol^{-1} , respectively, above the separated products. Intermediate **i1** can also isomerize via hydrogen atom migration to intermediates **i3** (-191 kJ mol^{-1}) and **i4** (-168 kJ mol^{-1}). Intermediate **i3** can undergo unimolecular decomposition via hydrogen atom elimination from the C2 carbon atom of the propylene moiety forming **p1** and **p2** (cis- and trans-1-propenyl-oxo-borane) through tight exit transition states. A competing methyl group elimination pathway from **i3** forms CH_2CHBO (**p5**) with an overall reaction exoergicity of 82 kJ mol^{-1} . The methyl loss channel proceeds through a tight exit transition state located 26 kJ mol^{-1} above the separated products. In the case of intermediate **i4**, the calculated energy barrier of the **i1 → i4** pathway is high (176 kJ mol^{-1}) with corresponding transition state residing only 5 kJ mol^{-1} below the energy of the separated reactants. Considering the associated energy barriers of the atomic hydrogen loss pathways from **i1**, the hydrogen migration pathway **i1 → i4** is expected to be less important due to the significantly higher barrier. The

statistical RRKM calculations (Supporting Information (SI) Table S2) also support the preceding statement as the rate constant of the reaction **i1 → i4** is at least 2 orders of magnitude lower than the rate constants for the decomposition pathways via atomic hydrogen loss to **p1**, **p2**, and **p3**. However, **i3** can isomerize to **i4** via [1,3] atomic hydrogen migration by overcoming an energy barrier of 171 kJ mol^{-1} . Subsequently, **i4** can undergo unimolecular decomposition via atomic hydrogen elimination from the C2 carbon atom to form **p3** by overcoming a tight exit transition state positioned 19 kJ mol^{-1} above the separated products.

Now, we discuss the reaction pathways associated with intermediate **i2** which can be formed either via the addition of the BO radical to the central carbon atom (C2) of the propylene reactant and/or [1,2] via BO migration from **i1**. Note that intermediate **i2** is only 21 kJ mol^{-1} less stable than **i1**, and these intermediates are connected via a [1,2] BO migration transition state placed 47 kJ mol^{-1} above **i2**. The above observations suggest a rapid **i1 ↔ i2** conversion which is in agreement with the rate constants calculated by statistical RRKM calculations (SI Table S2). Intermediate **i2** can undergo two competing unimolecular decomposition pathways via either an atomic hydrogen elimination from the C2 carbon atom of propylene to form $\text{CH}_3(\text{C}^{11}\text{BO})\text{CH}_2$ (**p4**) and/or methyl group elimination to form **p5**. Both reactions proceed via tight exit transition states residing 27 and 34 kJ mol^{-1} above the separated products, respectively. The formation of **p4** is exoergic by 39 kJ mol^{-1} with respect to the separated reactants. Intermediate **i2** can also isomerize via [1,2] hydrogen migration from the C2 carbon atom to either the C1 carbon atom to form **i5** (-208 kJ mol^{-1}) and/or to the B atom to form **i6** (-76 kJ mol^{-1}) which eventually undergoes atomic hydrogen elimination to form **p4**. The atomic hydrogen elimination reaction from **i5** and **i6** also proceeds via tight exit transition states positioned 7 and 11 kJ mol^{-1} , respectively, above the separated products. We found that **p4** formed via the reaction pathway through intermediate **i5** is the dominant reaction channel (91.0%) with minor contributions from the reaction pathways

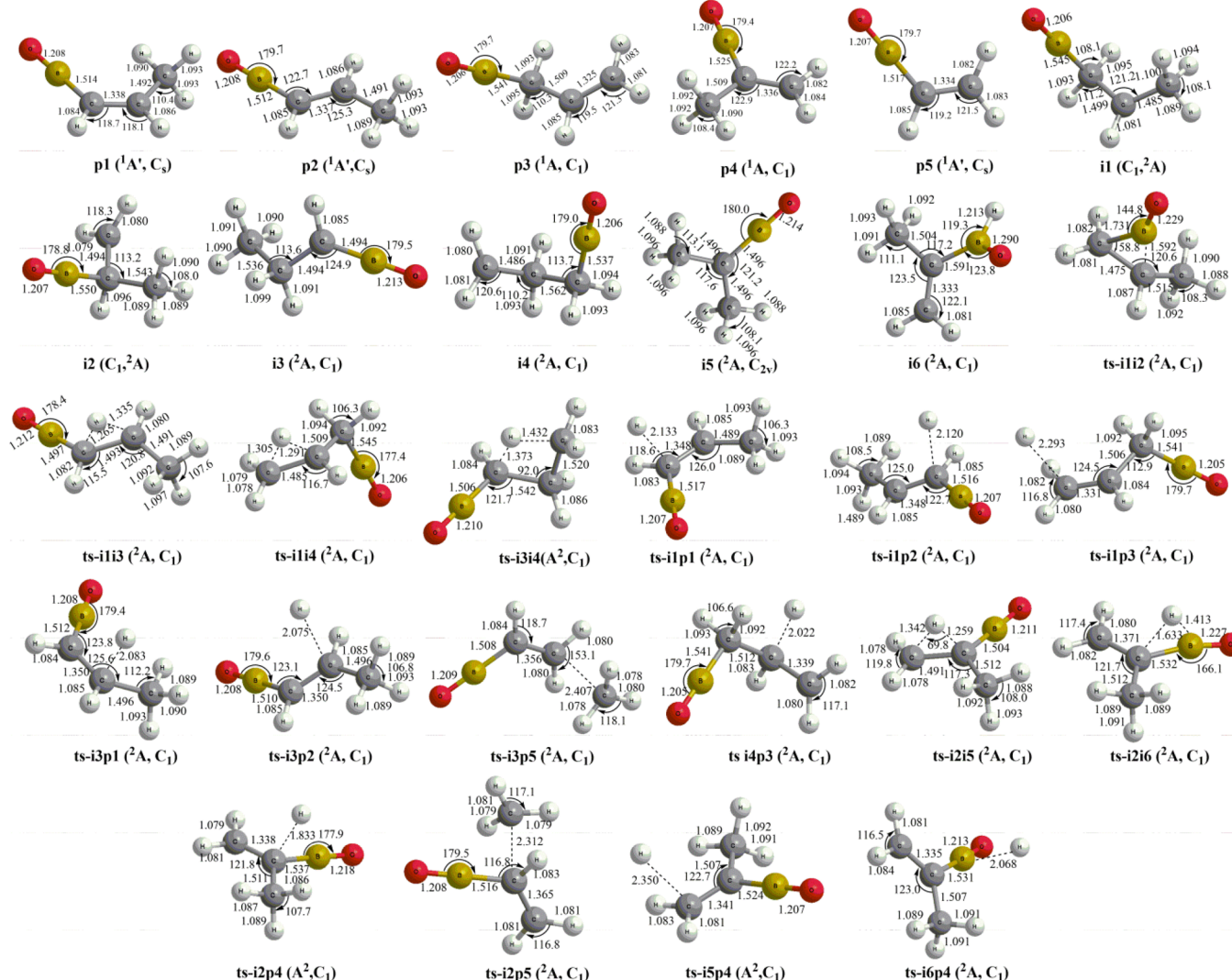


Figure 10. Structures of products, intermediates, and transition states relevant to the $^{11}\text{BOC}_3\text{H}_6$ PES. Angles and bond lengths are given in degrees and angstroms, respectively.

through intermediates **i2** (4.4%) and **i6** (4.6%) (SI Table S3). Here, intermediate **i5** (Figure 10) has C_{2v} symmetry since both methyl groups are identical. Therefore, an atomic hydrogen elimination from either of the methyl groups can lead to the formation of **p4**, implying that **p4** can be formed either via atomic hydrogen loss from the vinyl group or from the methyl group of propylene.

Statistical RRKM calculations have also been performed to predict the rate constants of each reaction pathway (SI Table S2) and eventually predict the branching ratios for the products (SI Table S3) at a collision energy of 22.5 kJ mol^{-1} . The branching ratios of the atomic hydrogen loss products **p1**, **p2**, **p3**, and **p4** are calculated to be 7.6%, 11.4%, 5.4%, and 0.8%, respectively; the branching ratio of the methyl group elimination product **p5** is the dominant product with a 74.9% yield. The branching ratios were calculated considering an initial 100% population of either **i1** or **i2**, and the calculated branching ratios of the products remain the same in both cases (SI Table S3).

6. DISCUSSION

In order to investigate the underlying reaction pathways and reaction dynamics involved in the reaction of $^{11}\text{BO}(X^2\Sigma^+)$ with $\text{CH}_3\text{CHCH}_2(X^1\text{A}')$, we are now comparing the experimental results with the theoretical data. First, let us briefly summarize the key experimental results (R1–R4).

(R1) The boron monoxide–propylene experiments suggest the existence of at least two competing reaction pathways: an atomic hydrogen loss and a methyl group elimination channel leading to $^{11}\text{BOC}_3\text{H}_5$ (68 amu) and $^{11}\text{BOC}_2\text{H}_3$ (54 amu) isomer(s), respectively, with relative fractions of $31 \pm 10\%$ and $69 \pm 15\%$, respectively. Experiments of boron monoxide with CD_3CHCH_2 and $\text{CH}_3\text{C}(\text{CD})_2$ clearly depict two distinct atomic hydrogen loss pathways from the vinyl and methyl groups leading to the formation of $^{11}\text{BOC}_3\text{D}_3\text{H}_2$ (71 amu) isomers, in each case, with fractions of $85 \pm 10\%$ and $15 \pm 10\%$, via atomic hydrogen versus boron monoxide exchange reactions.

(R2) The forward–backward symmetric center-of-mass angular distributions ($T(\theta)$) of both the atomic hydrogen and methyl loss pathways indicate indirect scattering dynamics via long-lived $^{11}\text{BOC}_3\text{H}_6$ collision complexes.

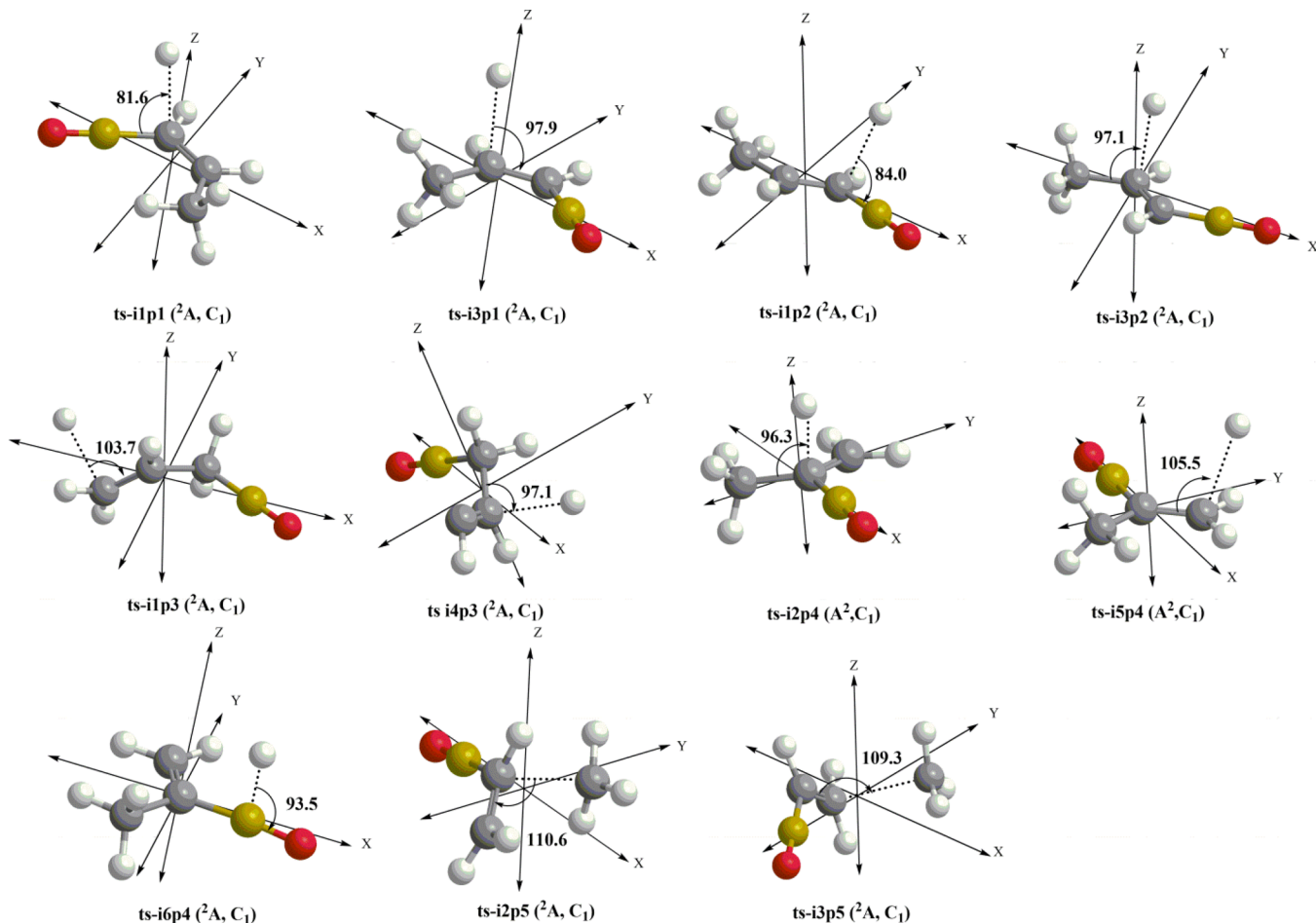


Figure 11. Geometry of the exit transition states relevant to the $^{11}\text{BOC}_3\text{H}_6$ PES. Angles are given in degrees.

(R3) The reaction exoergicities to form $^{11}\text{BOC}_3\text{H}_5$ (68 amu) and $^{11}\text{BOC}_2\text{H}_3$ (54 amu) isomers plus atomic hydrogen and the methyl group were determined to be 44 ± 12 and 69 ± 19 kJ mol $^{-1}$, respectively.

(R4) Both the atomic hydrogen and methyl loss pathways involve tight exit barriers in the order of 8–14 and 25–40 kJ mol $^{-1}$.

Here, we are now merging the experimental and computational results in order to identify the $^{11}\text{BOC}_3\text{H}_5$ (68 amu) and $^{11}\text{BOC}_2\text{H}_3$ (54 amu) isomers formed in the atomic hydrogen and methyl loss channels, respectively. From the electronic structure calculations, four different $^{11}\text{BOC}_3\text{H}_5$ isomers, **p1**, **p2**, **p3**, and **p4** can be formed with overall exoergicities of 47, 47, 32, and 39 kJ mol $^{-1}$, respectively. The cross molecular beam data verify a reaction exoergicity of 44 ± 12 kJ mol $^{-1}$. The experimental data agree with the computed reaction exoergicity of **p1** (-47 kJ mol $^{-1}$), **p2** (-47 kJ mol $^{-1}$), and **p4** (-39 kJ mol $^{-1}$). Note that, in the products **p1**, **p2**, and **p4**, one of the hydrogen atoms in the vinyl group (CHCH_2 group) of CH_3CHCH_2 is replaced by the boron monoxide radical. Recall that in the reaction of the boron monoxide radical with CD_3CHCH_2 , a predominant contribution ($85 \pm 10\%$) of atomic hydrogen loss from the vinyl group was determined experimentally. Based on the above observations, we can conclude that at least one of the products **p1**, **p2**, and/or **p4** is formed in the reaction between boron monoxide and propylene. However, we cannot exclude additional contributions from the thermodynamically less favorable product **p5**.

(-32 kJ mol $^{-1}$) based on the reaction exoergicity data alone. Further, the scattering reactions between the boron monoxide radical and CH_3CDCl_2 indicated that, to a minor amount ($15 \pm 10\%$), the hydrogen atom is lost from the methyl group. A comparison of the structures of the reactants with the $^{11}\text{BOC}_3\text{H}_5$ isomer **p3** shows that the ^{11}BO group adds at the C1 carbon atom and a subsequent hydrogen loss from the methyl group (C3 carbon atom) leads to the formation of the **p3**. Therefore, we can conclude that in the reaction between boron monoxide and propylene, products formed via atomic hydrogen elimination from the vinyl group dominates over the product formed via atomic hydrogen elimination from the methyl group with fractions of $85 \pm 15\%$ and $15 \pm 10\%$, respectively. In the case of the methyl loss channel, the computations predict only a single isomer $^{11}\text{BOC}_2\text{H}_3$ (54 amu), **p5**, with an overall exoergicity of 82 kJ mol $^{-1}$ which is in good agreement with the experimental finding of 69 ± 19 kJ mol $^{-1}$. Therefore, we can conclude that **p5** is the only $^{11}\text{BOC}_2\text{H}_3$ isomer formed in the boron monoxide versus methyl exchange pathway.

Having identified the products, we are now proposing the underlying reaction pathways by combining the experimental findings with the electronic structure and statistical calculations. A comparison of the structures of the reactants with the structures of the products suggests that the replacement of atomic hydrogen by boron monoxide radical leads to the products **p1–p4** and replacement of methyl group by boron monoxide radical leads to the product **p5**. Here, the reaction is

initiated by the barrierless addition of the boron monoxide radical with its radical center located on the boron atom to the C1 and possibly the C2 carbon atom of the propylene reactant resulting in the formation of $^{11}\text{BOC}_3\text{H}_6$ intermediates **i1** and **i2**, respectively. The initial BO addition to the C1 carbon atom is expected to be the dominant pathway compared to BO addition at the C2 carbon of propylene due to, *first*, the enhanced cone of acceptance at the C1 carbon compared to sterically crowded C2 carbon which is attached to the bulky methyl group³⁷ and, *second*, the concept of regioselectivity of electrophilic radical attacks on the unsaturated hydrocarbon molecules predicts that the addition is directed toward the carbon center that holds the highest spin density.⁷⁶ In the case of propylene, C1 carbon atom holds higher spin density (1.232) compared to C2 (1.216), suggesting a preferential addition of BO radical at the C1 carbon atom.⁷⁶ However, both intermediates can be easily interconverted due to the associated low energy barrier of 62/47 kJ mol⁻¹ with respect to **i1**/**i2**. Therefore, an initial addition of the boron monoxide radical (^{11}BO) to the terminal C1 carbon atom of CH_3CHCH_2 can easily isomerize to **i2** via ^{11}BO migration to the central carbon atom (C2) of propylene in agreement with the statistical RRKM calculations.

The unimolecular decomposition of **i1** via atomic hydrogen elimination from the vinyl group can lead to the formation of product **p1/p2**. The computations predict the presence of tight exit transition states located at 16 and 14 kJ mol⁻¹ above the separated products, respectively. These data agree with the experimental finding of the tight exit transition state suggested to reside 8–14 kJ mol⁻¹ above the separated products. A second reaction pathway, **i1** → **i3**, proceeds via [1,2] hydrogen atom migration from the C1 to the C2 carbon of propylene and can also form **p1/p2** via an atomic hydrogen loss from the C2 carbon (vinyl group). The associated tight exit transition states, located 17 kJ mol⁻¹ above the separated products, support the experimental findings of tight exit transition states. Further, the calculated geometry of these transition states (**ts-i1p1**, **ts-i1p2**, **ts-i3p1**, and **ts-i3p2**), as shown in Figure 11, connecting intermediates **i1**/**i3** and products **p1/p2**, suggest a direction of the atomic hydrogen emission almost perpendicularly ($90 \pm 8^\circ$) to the molecular plane. Recall that this geometry was predicted based on the shape (distribution maximum at 90°) of the center-of-mass angular distribution of the atomic hydrogen loss pathway (Figure 6). A comparison of the experimental findings and theoretical calculations suggests that **p1/p2** can be formed via atomic hydrogen elimination from both **i1** and/or **i3**. It becomes challenging to assign any preferential reaction pathways to **p1/p2** based on the experimental findings alone. Based on the $^{11}\text{BOC}_3\text{H}_6$ PES (Figure 9), the reaction pathways **i1** → **p1/p2** include a barrierless addition of boron monoxide to the C1 carbon of propylene followed by decomposition via atomic hydrogen elimination. On the other hand, pathways to **p1** and **p2** from **i3** are associated with the isomerization of **i1** by overcoming a large energy barrier of 145 kJ mol⁻¹. Second, **i3** exists exclusively via methyl elimination pathway to form the thermodynamically favorable product **p5** (see subsequent text). Therefore, the unimolecular decomposition of atomic hydrogen from the C1 carbon of **i1** is most likely the dominant reaction pathway to the formation of **p1/p2**. The statistical RRKM calculations support the above conclusions, and as shown in SI Table S3, 99.5% of the products **p1/p2** are formed via atomic hydrogen elimination from **i1** with only $\leq 0.5\%$ contributions from the hydrogen elimination from intermediate **i3**.

A competing unimolecular decomposition of **i1** via atomic hydrogen elimination from the methyl group can lead to the formation of **p3**. The computations predict the presence of tight exit transition states located at 9 kJ mol⁻¹ above the separated products supporting the experimental findings of a tight exit transition state. 3-Propenyl-oxo-borane can also be formed via atomic hydrogen loss elimination from **i4**. The reaction is associated with a tight exit transition state located 19 kJ mol⁻¹ above the separated products which positioned the transition state only 13 kJ mol⁻¹ below the separated reactants. Taking into account (i) a favorable position of the exit transition state **ts-i1p3** compared to **ts-i4p3** and (ii) the high energy barrier associated with the (multiple) hydrogen migrations from intermediate **i1** to form **i4**, we can suggest that the formation of **p3** most likely proceeds via atomic hydrogen elimination from the methyl group of intermediate **i1**. Once again, the statistical RRKM calculations support our prediction. Here, 99.8% of the product **p3** is formed via atomic hydrogen elimination from the methyl group of **i1** (SI Table S3).

Now we discuss the formation pathways of 2-propenyl-oxo-borane product, the only product showing an addition of BO to the central (C2) carbon of the propylene moiety. The above information suggests that **p4** can only be formed from intermediates related to **i2** where ^{11}BO is attached to the C2 carbon atom. Here, **i2** can undergo (i) unimolecular decomposition via atomic hydrogen loss, (ii) isomerization to form **i5** followed by decomposition via atomic hydrogen loss, and (iii) isomerization to form **i6** followed by decomposition via atomic hydrogen loss to form **p4** with the associated tight exit transition states located at 27, 7, and 11 kJ mol⁻¹ above the separated products. The reaction pathways **i2** → **p4** and **i2** → **i6** proceed through energy barriers of 154 and 153 kJ mol⁻¹, respectively, which are located only 12–13 kJ mol⁻¹ below the separated reactants. The above observation suggests that the reaction pathways **i2** → **p4** and **i2** → **i6** → **p4** are most likely the minor reaction channels to the formation of 2-propenyl-oxo-borane (**p4**). However, the favorable location of the associated transition states to the formation of **p4** via **i2** → **i5** → **p4** (31 and 32 kJ mol⁻¹ below the separated reactants) suggest this as a more favorable reaction pathway. The statistical RRKM calculations also support our preceding statement as the reaction pathway through intermediate **i5** is observed to be the dominant reaction channel (91.0%) compared to the reaction pathways through the intermediates **i2** (4.4%) and **i6** (4.6%).

Therefore, we can conclude that unimolecular decomposition via atomic hydrogen loss in the reaction of boron monoxide and propylene results in the formation of **p1/p2**, **p3**, and **p4**. Here, the dominant reaction pathways to form **p1/p2** and **p3** are found to be the unimolecular decomposition pathways via atomic hydrogen loss from the vinyl group (**p1/p2**) and the methyl group (**p3**) of the propylene moiety of intermediate **i1**. Among them, **p1/p2** are most likely the dominant hydrogen loss products due to the energetically favorable positions of the exit transition states [**ts-i1p1** (−31 kJ mol⁻¹), **ts-i1p2** (−33 kJ mol⁻¹) versus **ts-i1p3** (−23 kJ mol⁻¹)]. The statistical RRKM calculations also support the above statement and the dominant yield of **p1/p2** with a fraction of 76% of the total atomic hydrogen loss products; the contribution of **p3** is 21% of the total atomic hydrogen loss products. Recall that, from the reactions between boron monoxide radical and CD_3CHCH_2 and $\text{CH}_3\text{CDCCD}_2$, a predominant contribution ($85 \pm 10\%$) of

atomic hydrogen loss from the vinyl group and a minor contribution ($15 \pm 10\%$) of atomic hydrogen loss from the methyl group were experimentally determined. Our statistical RRKM calculations agree with the experimental findings with major contribution (76%) of atomic hydrogen loss from the vinyl group (**p1/p2**) and minor (21%) contribution from the methyl group (**p3**). Additional hydrogen loss channel to **p4** is found to be only 3%, and it can be formed via an atomic hydrogen loss either from the vinyl group and/or from the methyl group of the propylene moiety.

Finally we discuss the methyl group loss pathways to the formation of **p5**. The calculations support that intermediate **i2** can undergo unimolecular decomposition via methyl group loss to **p5**. This process involves a tight exit transition state located 34 kJ mol⁻¹ above the energy of the separated products. These data correlate very well with our experimental findings proposing a tight exit transition state located typically 25–40 kJ mol⁻¹ above the separated products. In addition, unimolecular decomposition via methyl group loss from **i3** can also lead to **p5**. The reaction proceeds through a tight exit transition state located 26 kJ mol⁻¹ above the separated products which is also in agreement to our experimental finding of 25–40 kJ mol⁻¹. The above facts conclude that both the methyl group elimination reaction pathways from **i2** and **i3** can lead to the formation of **p5**. Further, **i2** can be formed via either the direct ¹¹BO addition to the C2 carbon atom of propylene and/or rapid isomerization of **i1** by overcoming a low energy barrier of 62 kJ mol⁻¹. However, **i3** is formed by overcoming a high energy barrier of 145 kJ mol⁻¹. Although the rate constants (SI Table S2) of the reaction pathways **i2** → **p5** (5.45×10^8 s⁻¹) and **i3** → **p5** (4.93×10^8 s⁻¹), calculated using statistical RRKM calculations, are similar in magnitude, the methyl group elimination from **i2** is most likely the dominant reaction pathway considering its formation routes. The statistical RRKM calculations resulted in 94% of the **p5** being formed via methyl group loss from **i2** with only 6% formed via methyl group loss from **i3**.

Further, the rate constants obtained using statistical RRKM calculations show that the rate of the unimolecular decomposition via methyl loss from **i2** is 1 order of magnitude larger than the predominant reactions associated with the atomic hydrogen loss reaction channels (SI Table S2). This is most likely due to the favorable location of the exit transition state to **p5** positioned at 48 kJ mol⁻¹ below the separated reactants which is at least 15 kJ mol⁻¹ below the exit transition states related to the atomic hydrogen loss channels. The preceding facts reflect within the calculated branching ratio with a predominant (~75%) fraction of methyl loss product **p5** compared to minor (~25%) atomic hydrogen loss products. The above predictions also support our experimental findings of the atomic hydrogen loss and a methyl group elimination channel leading to ¹¹BOC₃H₅ (68 amu) and ¹¹BOC₂H₃ (54 amu) isomers, respectively, with relative fractions of $31 \pm 10\%$ and $69 \pm 15\%$, respectively.

In conclusion, the present studies propose that the reaction between ¹¹BO and propylene is initiated by barrierless addition of the ¹¹BO radical to the C1 and possibly C2 carbon atom of the propylene reactant leading to the formation of ¹¹BOC₃H₆ intermediates **i1** and **i2**, respectively. Intermediates **i1** and **i2** can isomerize quickly via low lying transition states. The methyl group elimination from **i2** to **p5** presents the thermodynamically most favorable pathway observed via both experiment ($69 \pm 15\%$) and theory (75%). An additional minor product

channel, proceeding via an atomic hydrogen migration from the C1 carbon atom to the C2 carbon atom of intermediate **i1** to form **i3**, undergoes unimolecular decomposition via exclusive methyl group loss to form **p5**. Intermediate **i1** fragments via three competing unimolecular decomposition pathways only via atomic hydrogen eliminations. Here, an elimination of atomic hydrogen from the vinyl group of the propylene moiety results in the dominant (experimental, $85 \pm 10\%$; calculated, 76%) ¹¹BO versus H exchange products **p1/p2** along with a minor product channel (experimental, $15 \pm 10\%$; calculated, 21%), where a hydrogen atom is lost from the methyl group. In addition, **p4**, which can be formed via an atomic hydrogen loss either from the vinyl group and/or from the methyl group of the propylene moiety, is found to be only 3%.

Here, we compare the results from the reactions of ¹¹BO(X^{2Σ⁺}) and CN(X^{2Σ⁺}) radicals with propylene as the boron monoxide radical remains an interesting system from the physical organic chemistry viewpoint because of the isoelectronic character of these two radicals. The reactions between propylene and the cyano radical were previously investigated via both experimental³⁷ and theoretical analysis.⁷⁷ Here, both reactions undergo indirect scattering dynamics via defacto barrierless additions of the radical to the C1 and/or C2 carbon atoms of the propylene reactant leading to CH₃CHCH₂X and (CH₃)XCHCH₂ doublet reaction intermediates (X = BO, CN), respectively. These doublet radical intermediates are stabilized by 223–233 kJ mol⁻¹ (X = CN) and 166–181 kJ mol⁻¹ (X = BO), and these energetics indicate the formation of a stronger carbon–carbon (X = CN) bond compared to a weaker carbon–boron (X = BO) single bond; bond strengths differ by typically 50 kJ mol⁻¹. For both systems, the atomic hydrogen elimination channels lead to four distinct isomers of substituted propylene with general formula *cis/trans* CH₃CHCH₂X, CH₂CHCH₂X, and CH₃C(X)CH₂ (X = CN, BO). The X (CN, BO) versus H exchange reactions between X (BO, CN) radical with CD₃CHCH₂ and CH₃CD₂, i.e., the atomic hydrogen loss from the vinyl group and methyl group, are observed with fractions of about $85 \pm 10\%$ versus $15 \pm 10\%$ (BO reaction) and $75 \pm 8\%$ versus $25 \pm 5\%$ (CN reaction), respectively. Also, the decomposition pathways involve tight exit transition states located 8–14 kJ mol⁻¹ (X = BO) and 30–40 kJ mol⁻¹ (X = CN) above the separated products, and the substituted propylene products *cis/trans* CH₃CHCH₂X, CH₂CHCH₂X, and CH₃C(X)CH₂ (X = CN, BO) are formed in exoergic reactions (X = BO, 32–47 kJ mol⁻¹; X = CN, 80–104 kJ mol⁻¹). The enhanced exoergicity of the cyano radical reaction products is likely due to the effect of an enhanced carbon–carbon bond strength compared to the weaker carbon–boron single bond strength. Additionally, both reactions should yield the thermodynamically most favorable methyl loss pathway forming substituted ethylene product CH₂CHX (X = BO, CN). The present study clearly demonstrated the dominant methyl loss pathway, whereas the methyl loss elimination could not be observed in the CN + propylene reaction. Here, ground state atomic carbon reacts with propylene molecule leading to C₄H₅ isomers (53 amu) plus atomic hydrogen.⁷⁸ On the other hand, the associated methyl loss channel in the CN + propylene reaction forms cyanoethylene (CH₂CHCN) with mass-to-charge ratio of 53 amu. Considering that the atomic carbon reactant has a much higher concentration in the interaction region of the scattering chamber compared to the cyano radical reactant by a factor of about 20, the signal at *m/z* = 53 is dominated by C₄H₅ ions.⁷⁹

Future studies of the cyano–propylene system should exploit photolytically generated supersonic cyano radical beams such as from bromo or iodocyanide or cyanogen (NCCN) to probe the methyl loss pathway.

In addition, we compare the present results with the $^{11}\text{BO}(\text{X}^2\Sigma^+) - \text{CH}_3\text{CCH}(\text{X}^1\text{A}_1)$ system studied previously in our group.²⁶ The reaction of the ^{11}BO radical with methylacetylene undergoes indirect scattering dynamics and is initiated by the formation of a van der Waals complex, which eventually isomerizes via the addition of a ^{11}BO radical to the carbon–carbon triple bond of methylacetylene at the C1 and/or C2 carbon center. Here, the doublet intermediates $^{11}\text{BOC}_3\text{H}_4$ are stabilized by $170\text{--}197\text{ kJ mol}^{-1}$ with respect to the reactants similar to the present $^{11}\text{BOC}_3\text{H}_6$ doublet intermediates ($166\text{--}181\text{ kJ mol}^{-1}$). In addition, the intermediates underwent decomposition via competing atomic hydrogen and methyl group loss pathways with the methyl loss pathway being with $56\pm15\%$ (methylacetylene) and $69\pm15\%$ (propylene). Another striking similarity between the product channels are the observed branching ratios between the competing atomic hydrogen loss pathways. In the case of the ^{11}BO –methylacetylene system, the dominant acetylenic hydrogen atom loss (from C1 carbon atom) results in the formation of $1\text{-CH}_3\text{CC}^{11}\text{BO}$ (-71 kJ mol^{-1}) along with a smaller fraction of an atomic hydrogen loss from the methyl group ($\text{CH}_2(^{11}\text{BO})\text{CCH}$; -43 kJ mol^{-1}) with a ratio of $90\pm5\%$ versus $10\pm5\%$, respectively. Recall that, in the present system, the atomic hydrogen loss from the BO addition center, i.e. C1 and C2 carbon atoms are $85\pm10\%$ compared to the atomic hydrogen loss from the methyl group ($15\pm10\%$). However, the reaction energy of the dominant atomic hydrogen loss product in the methylacetylene system ($\text{CH}_3\text{CC}^{11}\text{BO}$; -71 kJ mol^{-1}) is about 24 kJ mol^{-1} higher than the present propylene system (*cis-/trans-* $\text{CH}_3\text{CHCH}^{11}\text{BO}$; -47 kJ mol^{-1}), most likely due to the stabilization of ^{11}BO substituted methylacetylene via a conjugated triple bond. The difference in reaction energies also agrees with the difference observed in the case of $\text{BO} + \text{C}_2\text{H}_2$ and $\text{BO} + \text{C}_2\text{H}_4$ reactions, where the products were HCC^{11}BO (-57 kJ mol^{-1}) and $\text{H}_2\text{CCH}^{11}\text{BO}$ (-39 kJ mol^{-1}), respectively.^{24,25}

7. SUMMARY

The crossed molecular beam reaction of boron monoxide ($^{11}\text{BO}; \text{X}^2\Sigma^+$) with propylene ($\text{CH}_3\text{CHCH}_2; \text{X}^1\text{A}'$) was investigated at a collision energy of $22.5\pm1.3\text{ kJ mol}^{-1}$ under single collision conditions and was correlated with *ab initio* electronic structure calculations and RRKM calculations. The scattering dynamics were found to be indirect and proceeded via barrierless addition of boron monoxide radical with its radical center located at the boron atom to either the terminal carbon atom (C1) and/or the central carbon atom (C2) of CH_3CHCH_2 reactant forming $^{11}\text{BOC}_3\text{H}_6$ intermediates. The resulting $^{11}\text{BOC}_3\text{H}_6$ doublet radical intermediates underwent unimolecular decomposition involving at least three competing reaction mechanisms via atomic hydrogen loss from the vinyl and the methyl groups of propylene and a methyl group elimination. The hydrogen atom elimination from the vinyl group of propylene can lead to the formation of *cis-/trans-*1-propenyl-oxo-borane ($\text{CH}_3\text{CHCH}^{11}\text{BO}$) whereas a hydrogen atom elimination from the methyl group of propylene can lead to the formation of 3-propenyl-oxo-borane ($\text{CH}_2\text{CHCH}_2^{11}\text{BO}$). An additional minor reaction channel to

form 2-propenyl-oxo-borane ($\text{CH}_3\text{C}^{(11}\text{BO})\text{CH}_2$) can be formed via atomic hydrogen loss from either of the vinyl group and the methyl group. Combined with theoretical results, the experiment results suggested that all of the products were formed in exoergic reactions by overcoming tight exit transition states. Utilizing partially deuterated propylene reactants (CD_3CHCH_2 and CH_3CDCH_2), we revealed that the loss of vinyl hydrogen atom was the dominating hydrogen elimination pathway ($85\pm10\%$) compared to the loss of methyl hydrogen atom ($15\pm10\%$). Further, the addition of $^{11}\text{BO}(\text{X}^2\Sigma^+)$ to the C2 carbon atom of propylene and/or addition of $^{11}\text{BO}(\text{X}^2\Sigma^+)$ to the C1 carbon atom followed by ^{11}BO migration to the C2 carbon atom of propylene underwent unimolecular decomposition via a methyl group loss leading to the formation of the product ethenyl-oxo-borane ($\text{CH}_2\text{CH}^{11}\text{BO}$) via an overall exoergic reaction ($69\pm19\text{ kJ mol}^{-1}$). The branching ratios for atomic hydrogen loss from the vinyl group, atomic hydrogen loss from the methyl group, and the methyl group loss were derived to be $26\pm8\%$, $5\pm3\%$, $69\pm15\%$, respectively, which are in agreement with the branching ratios calculated using statistical RRKM theory yielding 19%, 5%, and 75%, respectively.

■ ASSOCIATED CONTENT

S Supporting Information

Relative energies with respect to the reactants in kilojoules per mole (Table S1) and Cartesian coordinates (Å; Table S4) of reactants, intermediates, products, and transition states optimized at the CCSD(T)/cc-pVTZ level of theory, the rate constant of each reaction pathway (Table S2), and branching ratios of the products (Table S3) calculated using statistical RRKM theory at the collision energy of 22.5 kJ mol^{-1} . This material is available free of charge via the Internet at <http://pubs.acs.org>.

■ AUTHOR INFORMATION

Notes

The authors declare no competing financial interest.

■ ACKNOWLEDGMENTS

This work was supported by the Air Force Office of Scientific Research, Grant FA9550-12-1-0213. Computer resources at the National Center for High Performance Computer of Taiwan were utilized in the calculations.

■ REFERENCES

- (1) Young, G.; Sullivan, K.; Zacharia, M. R.; Yu, K. Combustion Characteristic of Boron Nanoparticles. *Combust. Flame* **2009**, *156*, 322–333.
- (2) Ulas, A.; Kuo, K. K.; Gotzmer, C. Ignition and Combustion of Boron Particles in Fluorine Containing Environment. *Combust. Flame* **2001**, *127*, 1935–1957.
- (3) Hinchen, J. J. Kinetics for the Quenching and Relaxation of Boron Oxide. *J. Chem. Phys.* **1993**, *99*, 4403–4410.
- (4) Yeh, C. L.; Kuo, K. K. Ignition and Combustion of Boron Particles. *Prog. Energy Combust. Sci.* **1996**, *22*, 511–541.
- (5) Turns, S. R.; Holl, J. T.; Solomon, A. S. P.; Faeth, G. M. Gasification of Boron Oxide Drops in Combustion Gases. *Combust. Sci. Technol.* **1985**, *43*, 287–300.
- (6) Li, S. C.; Williams, F. A. Combustion of Boron-Based Solid Propellants and Solid Fuels. In *Combustion of Boron-Based Solid Propellants and Solid Fuels*; Kuo, K. K., Pein, R., Eds.; CRC Press: Boca Raton, FL, USA, 1993; p 248.

- (7) Macek, A. Combustion of Boron Particles: Experiments and Theory. *Proc. Combust. Inst.* **1972**, *14*, 1401–1411.
- (8) King, M. K. Ignition and Combustion of Boron Particles and Clouds. *J. Spacecr. Rockets* **1982**, *19*, 294–306.
- (9) Zhou, W.; Yetter, R. A.; Dryer, F. L.; Rabitz, H.; Brown, R. C.; Kolb, C. E. Multi-Phase Model for Ignition and Combustion of Boron Particles. *Combust. Flame* **1999**, *117*, 227–243.
- (10) Yetter, R.; Rabitz, H.; Dryer, F.; Brown, R.; Kolb, C. Kinetics of High-Temperature B/O/H/C Chemistry. *Combust. Flame* **1991**, *83*, 43–62.
- (11) Yetter, R.; Dryer, F.; Rabitz, H. A Comprehensive Reaction Mechanism for Carbon Monoxide/Hydrogen/Oxygen Kinetics. *Combust. Sci. Technol.* **1991**, *79*, 97–128.
- (12) Brown, R. C.; Kolb, C. E.; Yetter, R. A.; Dryer, F. L.; Rabitz, H. Kinetic Modeling and Sensitivity Analysis for B/H/O/C/F Combination Systems. *Combust. Flame* **1995**, *101*, 221–238.
- (13) Hussmann, B.; Pfitzner, M. Extended Combustion Model for Single Boron Particles—Part II: Validation. *Combust. Flame* **2010**, *157*, 822–833.
- (14) Hussmann, B.; Pfitzner, M. Extended Combustion Model for Single Boron Particles - Part I: Theory. *Combust. Flame* **2010**, *157*, 803–821.
- (15) Balucani, N.; Zhang, F.; Kaiser, R. I. Elementary Reactions of Boron Atoms with Hydrocarbons—Toward the Formation of Organo-Boron Compounds. *Chem. Rev.* **2010**, *110*, 5107–5127.
- (16) Zhang, F.; Gu, X.; Kaiser, R. I.; Bettinger, H. A Reinvestigation of the Gas Phase Reaction of Boron Atoms, $^{11}\text{B}({}^2\text{P}_j)/{}^{10}\text{B}({}^2\text{P}_j)$ with Acetylene, C_2H_2 ($\text{X}^1\Sigma_g^+$). *Chem. Phys. Lett.* **2007**, *450*, 178–185.
- (17) Zhang, F.; Gu, X.; Kaiser, R. I.; Balucani, N.; Huang, C. H.; Kao, C. H.; Chang, A. H. H. A Crossed Beam and ab Initio Study of the Reaction of Atomic Boron with Ethylene. *J. Phys. Chem. A* **2008**, *112*, 3837–3845.
- (18) Zhang, F.; Kao, C. H.; Chang, A. H. H.; Gu, X.; Guo, Y.; Kaiser, R. I. A Crossed Molecular Beam Study on the Reaction of Boron Atoms with Methylacetylene and Partially Deuterated Methylacetylene. *ChemPhysChem* **2008**, *9*, 95–105.
- (19) Zhang, F.; Sun, H. L.; Chang, A. H. H.; Gu, X.; Kaiser, R. I. Crossed Molecular Beam Study on the Reaction of Boron Atoms, $\text{B}({}^2\text{P}_j)$, with Allene, $\text{H}_2\text{CCCH}_2(\text{X}^1\text{A}_1)$. *J. Phys. Chem. A* **2007**, *111*, 13305–13310.
- (20) Sillars, D.; Kaiser, R. I.; Galland, N.; Hannachi, Y. Crossed-Beam Reaction of Boron Atoms, $\text{B}({}^2\text{P}_j)$, with Dimethylacetylene, CH_3CCCH_3 (X^1A_{1g}): Untangling the Reaction Dynamics to Form the 1,2-Dimethylene-3-bora-cyclopropane Molecule. *J. Phys. Chem. A* **2003**, *107*, 5149–5156.
- (21) Zhang, F.; Guo, Y.; Gu, X.; Kaiser, R. I. A Crossed Molecular Beam Study on the Reaction of Boron Atoms, $\text{B}({}^2\text{P}_j)$, with Benzene, $\text{C}_6\text{H}_6(\text{X}^1\text{A}_{1g})$, and D6-Benzene $\text{C}_6\text{D}_6(\text{X}^1\text{A}_{1g})$. *Chem. Phys. Lett.* **2007**, *440*, 56–63.
- (22) Bauer, S. H. Oxidation of B , BH , BH_2 , and B_mH_n Species: Thermochemistry and Kinetics. *Chem. Rev.* **1996**, *96*, 1907–1916.
- (23) Brown, R. C.; Kolb, C. E.; Rabitz, H.; Cho, S. Y.; Yetter, R. A.; Dryer, F. L. Kinetic Model of Liquid B_2O_3 Gasification in a Hydrocarbon Combustion Environment: I. Heterogeneous Surface Reaction. *Int. J. Chem. Kinet.* **1991**, *23*, 957–970.
- (24) Parker, D. S. N.; Zhang, F.; Maksyutenko, P.; Kaiser, R. I.; Chang, A. H. H. A Crossed Beam and Ab Initio Investigation of the Reaction of Boron Monoxide (BO) with Acetylene (C_2H_2). *Phys. Chem. Chem. Phys.* **2011**, *13*, 8560–8570.
- (25) Parker, D. S. N.; Zhang, F.; Maksyutenko, P.; Kaiser, R. I.; Chen, S. H.; Chang, A. H. H. A Crossed Beam and Ab Initio Investigation on the Formation of Vinyl Boron Monoxide ($\text{C}_2\text{H}_3\text{BO}$) Via Reaction of Boron Monoxide (BO) with Ethylene (C_2H_4). *Phys. Chem. Chem. Phys.* **2012**, *14*, 11099–11106.
- (26) Maity, S.; Parker, D. S. N.; Dangi, B. B.; Kaiser, R. I.; Fau, S.; Perera, A.; Bartlett, R. J. A Crossed Molecular Beam and Ab-Initio Investigation of the Reaction of Boron Monoxide (BO; $\text{X}^2\Sigma^+$) with Methylacetylene (CH_3CCH ; X^1A_1): Competing Atomic Hydrogen and Methyl Loss Pathways. *J. Phys. Chem. A* **2013**, *117*, 11794–11807.
- (27) Kaiser, R. I.; Maity, S.; Dangi, B. B.; Su, Y.-S.; Sun, B. J.; Chang, A. H. H. A Crossed Molecular Beam and Ab Initio Investigation of the Exclusive Methyl Loss Pathway in the Gas Phase Reaction of Boron Monoxide (BO; $\text{X}^2\Sigma^+$) with Dimethylacetylene (CH_3CCCH_3 ; X^1A_{1g}). *Phys. Chem. Chem. Phys.* **2014**, *16*, 989–997.
- (28) Parker, D. S. N.; Balucani, N.; Stranges, D.; Kaiser, R. I.; Mebel, A. M. A Crossed Beam and ab Initio Investigation on the Formation of Boronyldiacetylene ($\text{HCCCC}^{11}\text{BO}$; $\text{X}^1\Sigma^+$) via the Reaction of the Boron Monoxide Radical (^{11}BO ; $\text{X}^2\Sigma^+$) with Diacetylene (C_4H_2 ; $\text{X}^1\Sigma_g^+$). *J. Phys. Chem. A* **2013**, *117*, 8189–8198.
- (29) Parker, D. S. N.; Dangi, B. B.; Balucani, N.; Stranges, D.; Mebel, A. M.; Kaiser, R. I. Gas-Phase Synthesis of Phenyl Oxborane ($\text{C}_6\text{H}_5\text{BO}$) via the Reaction of Boron Monoxide with Benzene. *J. Org. Chem.* **2013**, *78*, 11896–11900.
- (30) Li, S.-D.; Guo, J.-C.; Ren, G.-M. Density Functional Theory Investigations on Boronyl-Substituted Ethylenes $\text{C}_2\text{H}_4\text{-m(BO)M}$ ($m = 1–4$) and Acetylenes $\text{C}_2\text{H}_2\text{-m(BO)M}$ ($m = 1, 2$). *J. Mol. Struct.* **2007**, *821*, 153–159.
- (31) Ollivier, C.; Renaud, P. Organoboranes as a Source of Radicals. *Chem. Rev.* **2001**, *101*, 3415–3434.
- (32) Papakondylis, A.; Mavridis, A. Structure and Bonding of the Polytopic Molecule $\text{Li}[\text{BO}]$. A Theoretical Investigation. *J. Phys. Chem. A* **2001**, *105*, 7106–7110.
- (33) Zhai, H.-J.; Li, S.-D.; Wang, L.-S. Boronyls as Key Structural Units in Boron Oxide Clusters: $\text{B}(\text{BO})_2$ - and $\text{B}(\text{BO})_3$. *J. Am. Chem. Soc.* **2007**, *129*, 9254–9255.
- (34) Huang, L. C. L.; Asvany, O.; Chang, A. H. H.; Balucani, N.; Lin, S. H.; Lee, Y. T.; Kaiser, R. I.; Osamura, Y. Crossed Beam Reaction of Cyano Radicals with Hydrocarbon Molecules. IV. Chemical Dynamics of Cyanoacetylene (HCCCN ; $\text{X}^1\Sigma^+$) Formation from Reaction of $\text{CN}(\text{X}^2\Sigma^+)$ with Acetylene, $\text{C}_2\text{H}_2(\text{X}^1\Sigma_g^+)$. *J. Chem. Phys.* **2000**, *113*, 8656–8666.
- (35) Balucani, N.; Asvany, O.; Chang, A. H. H.; Lin, S. H.; Lee, Y. T.; Kaiser, R. I.; Osamura, Y. Crossed Beam Reaction of Cyano Radicals with Hydrocarbon Molecules. III. Chemical Dynamics of Vinyl Cyanide ($\text{C}_2\text{H}_3\text{CN}; \text{X}^1\text{A}'$) Formation from Reaction of $\text{CN}(\text{X}_2\Sigma^+)$ with Ethylene, $\text{C}_2\text{H}_4(\text{X}^1\text{A}_g)$. *J. Chem. Phys.* **2000**, *113*, 8643–8655.
- (36) Huang, L. C. L.; Balucani, N.; Lee, Y. T.; Kaiser, R. I.; Osamura, Y. Crossed Beam Reaction of the Cyano Radical, $\text{CN}(\text{X}^2\Sigma^+)$, with Methylacetylene, CH_3CCH (X^1A_1): Observation of Cyanopropyne, CH_3CCCN (X^1A_1), and Cyanoallene, H_2CCCHCN ($\text{X}^1\text{A}'$). *J. Chem. Phys.* **1999**, *111*, 2857–2860.
- (37) Gu, X.; Zhang, F.; Kaiser, R. I. Reaction Dynamics on the Formation of 1- and 3-Cyanopropylene in the Crossed Beams Reaction of Ground-State Cyano Radicals (CN) with Propylene (C_3H_6) and Its Deuterated Isotopologues. *J. Phys. Chem. A* **2008**, *112*, 9607–9613.
- (38) Balucani, N.; Asvany, O.; Chang, A. H. H.; Lin, S. H.; Lee, Y. T.; Kaiser, R. I.; Bettinger, H. F.; Schleyer, P. v. R.; Schaefer, H. F., III. Crossed Beam Reaction of Cyano Radicals with Hydrocarbon Molecules. II. Chemical Dynamics of 1-Cyano-1-Methylallene ($\text{CNCH}_3\text{CCCH}_2$; $\text{X}^1\text{A}'$) Formation from Reaction of $\text{CN}(\text{X}^2\Sigma^+)$ with Dimethylacetylene, CH_3CCCH_3 ($\text{X}^1\text{A}_1'$). *J. Chem. Phys.* **1999**, *111*, 7472–7479.
- (39) Balucani, N.; Asvany, O.; Chang, A. H. H.; Lin, S. H.; Lee, Y. T.; Kaiser, R. I.; Bettinger, H. F.; Schleyer, P. v. R.; Schaefer, H. F., III. Crossed Beam Reaction of Cyano Radicals with Hydrocarbon Molecules. I. Chemical Dynamics of Cyanobenzene ($\text{C}_6\text{H}_5\text{CN}$; X^1A_1) and Perdeutero Cyanobenzene ($\text{C}_6\text{D}_5\text{CN}$; X^1A_1) Formation from Reaction of $\text{CN}(\text{X}^2\Sigma^+)$ with Benzene, $\text{C}_6\text{H}_6(\text{X}^1\text{A}_{1g})$, and D6-Benzene, $\text{C}_6\text{D}_6(\text{X}^1\text{A}_{1g})$. *J. Chem. Phys.* **1999**, *113*, 7457–7471.
- (40) Kaiser, R. I.; Balucani, N. The Formation of Nitriles in Hydrocarbon-Rich Atmospheres of Planets and Their Satellites: Laboratory Investigations by the Crossed Molecular Beam Technique. *Acc. Chem. Res.* **2001**, *34*, 699–706.
- (41) Fischer, R. C.; Power, P. P. Π -Bonding and the Lone Pair Effect in Multiple Bonds Involving Heavier Main Group Elements: Developments in the New Millennium. *Chem. Rev.* **2010**, *110*, 3877–3923.

- (42) Wang, Y.; Hu, H.; Zhang, J.; Cui, C. Comparison of Anionic and Lewis Acid Stabilized N-Heterocyclic Oxaboranes: Their Facile Synthesis from a Borinic Acid. *Angew. Chem., Int. Ed.* **2011**, *50*, 2816–2819.
- (43) Kawashima, Y.; Endo, E.; Kawaguchi, K.; Hirota, E. Detection and Equilibrium Molecular Structure of a Short-Lived Molecule, HBO, by Microwave Spectroscopy. *Chem. Phys. Lett.* **1987**, *135*, 441–445.
- (44) Lanzisera, D. V.; Andrews, L. Reactions of Laser-Ablated Boron Atoms with Methanol. Infrared Spectra and *ab Initio* Calculations of CH_3BO , CH_2BOH , and CH_2BO in Solid Argon. *J. Phys. Chem. A* **1997**, *101*, 1482–1487.
- (45) Andrews, L.; Burkholder, T. R. Infrared Spectra of Boron Atom-Water Molecule Reaction Products Trapped in Solid Argon. *J. Phys. Chem.* **1991**, *95*, 8554–8560.
- (46) Bettinger, H. F. Reversible Formation of Organyl(Oxo)Boranes (RBO) ($\text{R} = \text{C}_6\text{H}_5$ or CH_3) from Boroxins ((RBO)₃): A Matrix Isolation Study. *Organometallics* **2007**, *26*, 6263–6267.
- (47) Pachaley, B.; West, R. Synthesis of a 1,3-Dioxa-2,4-Diboretane, an Oxaborane Precursor. *J. Am. Chem. Soc.* **1985**, *107*, 2987–2988.
- (48) Ito, M.; Tokitoh, N.; Okazaki, R. A Novel Approach to an Oxaborane and Its Lewis Base Complex. *Tetrahedron Lett.* **1997**, *38*, 4451–4454.
- (49) Bock, H.; Cederbaum, L.; Niessen, W. v.; Paezzold, P.; Rosmus, P.; Solouki, B. Methylboron Oxide, $\text{H}_3\text{C}-\text{B}\equiv\text{O}$. *Angew. Chem., Int. Ed.* **1989**, *28*, 88–90.
- (50) Braunschweig, H.; Radacki, K.; Schneider, A. Oxboryl Complexes: Boron–Oxygen Triple Bonds Stabilized in the Coordination Sphere of Platinum. *Science* **2010**, *328*, 345–347.
- (51) Braunschweig, H.; Radacki, K.; Schneider, A. Cyclodimerization of an Oxboryl Complex Induced by Trans Ligand Abstraction. *Angew. Chem., Int. Ed.* **2010**, *49*, 5993–5996.
- (52) Chang, Y.; Li, Q.-S.; Xie, Y.; King, R. B.; Schaefer, H. F., III. Binuclear Iron Boronyl Carbonyls Isoelectronic with the Well-Known Decacarbonyldimanganese. *New J. Chem.* **2012**, *36*, 1022–1030.
- (53) Chang, Y.; Li, Q.-S.; Xie, Y.; King, R. B. Prospects for Three-Electron Donor Boronyl (BO) Ligands and Dioxodiborene (B_2O_2) Ligands as Bridging Groups in Binuclear Iron Carbonyl Derivatives. *Inorg. Chem.* **2012**, *51*, 8904–8915.
- (54) Gu, X.; Guo, Y.; Zhang, F.; Mebel, A. M.; Kaiser, R. I. Reaction Dynamics of Carbon-Bearing Radicals in Circumstellar Envelopes of Carbon Stars. *Faraday Discuss.* **2006**, *133*, 245–275.
- (55) Gu, X.; Guo, Y.; Kaiser, R. I. Mass Spectrum of the Butadiynyl Radical ($\text{C}_4\text{H}; \text{X}^2 \Sigma^+$). *Int. J. Mass Spectrom.* **2005**, *246*, 29–34.
- (56) Gu, X. B.; Guo, Y.; Kawamura, E.; Kaiser, R. I. Design of a Convection-Cooled, Cluster-Based Voltage Divider Chain for Photomultiplier Tubes. *Rev. Sci. Instrum.* **2005**, *76*, No. 083115.
- (57) Guo, Y.; Gu, X.; Kaiser, R. I. Mass Spectrum of the 1-Butene-3-yne-2-yl Radical ($\text{I-C}_4\text{H}_3; \text{X}^2 \text{A}'$). *Int. J. Mass Spectrom.* **2006**, *249/250*, 420–425.
- (58) Guo, Y.; Gu, X.; Kawamura, E.; Kaiser, R. I. Design of a Modular and Versatile Interlock System for Ultrahigh Vacuum Machines: A Crossed Molecular Beam Setup as a Case Study. *Rev. Sci. Instrum.* **2006**, *77*, No. 034701.
- (59) Gu, X.; Guo, Y.; Kawamura, E.; Kaiser, R. I. Characteristics and Diagnostics of an Ultrahigh Vacuum Compatible Laser Ablation Source for Crossed Molecular Beam Experiments. *J. Vac. Sci. Technol., A* **2006**, *24*, 505–511.
- (60) Proch, D.; Trickl, T. A High-Intensity Multi-Purpose Piezoelectric Pulsed Molecular Beam Source. *Rev. Sci. Instrum.* **1989**, *60*, 713–716.
- (61) Maksyutenko, P.; Parker, D. S. N.; Zhang, F.; Kaiser, R. I. An LIF Characterization of Supersonic BO and CN Radical Sources for Crossed Beam Studies. *Rev. Sci. Instrum.* **2011**, *82*, No. 083107.
- (62) Tan, X. *CyberWit Diatomic*, Version 1.4.1.1; CyberWit Software Solutions: 2004.
- (63) Vernon, M. LBL Report-12422, 1981.
- (64) Weis, P. S. Ph.D. Thesis, University of California, Berkley, 1986.
- (65) Krajnovich, D.; Huisken, F.; Zhang, Z.; Shen, Y. R.; Lee, Y. T. Competition between Atomic and Molecular Chlorine Elimination in the Infrared Multiphoton Dissociation of CF_2Cl_2 . *J. Chem. Phys.* **1982**, *77*, 5977–5989.
- (66) Becke, A. D. Density-Functional Thermochemistry. III. The Role of Exact Exchange. *J. Chem. Phys.* **1993**, *98*, 5648–5652.
- (67) Lee, C.; Yang, W.; Parr, R. G. Development of the Colle-Salvetti Correlation-Energy Formula into a Functional of the Electron Density. *Phys. Rev. B: Condens. Matter Mater. Phys.* **1988**, *37*, 785–789.
- (68) Deegan, M. J. O.; Knowles, P. J. Perturbative Corrections to Account for Triple Excitations in Closed and Open Shell Coupled Cluster Theories. *Chem. Phys. Lett.* **1994**, *227*, 321–326.
- (69) Hampel, C.; Peterson, K. A.; Werner, H. J. A Comparison of the Efficiency and Accuracy of the Quadratic Configuration Interaction (QCISD), Coupled Cluster (CCSD), and Brueckner Coupled Cluster (BCCD) Methods. *Chem. Phys. Lett.* **1992**, *190*, 1–12.
- (70) Knowles, P. J.; Hampel, C.; Werner, H. J. Coupled Cluster Theory for High Spin, Open Shell Reference Wave Functions. *J. Chem. Phys.* **1993**, *99*, 5219–5227.
- (71) Purvis, G. D., III; Bartlett, R. J. A Full Coupled-Cluster Singles and Doubles Model: The Inclusion of Disconnected Triples. *J. Chem. Phys.* **1982**, *76*, 1910–1918.
- (72) Frisch, M. J.; Trucks, G. W.; Schlegel, H. B.; Scuseria, G. E.; Robb, M. A.; Cheeseman, J. R.; Zakrzewski, V. G.; Montgomery, J. A.; Stratmann, R. E.; Burant, J. C.; et al.; *Gaussian 03*, Revision C.02; Gaussian: Wallingford, CT, USA, 2004.
- (73) Chang, A. H. H.; Mebel, A. M.; Yang, X. M.; Lin, S. H.; Lee, Y. T. Ab Initio/RRKM Approach toward the Understanding of Ethylene Photodissociation. *J. Chem. Phys.* **1998**, *109*, 2748–2761.
- (74) Kaiser, R. I.; Mebel, A. M. The Reactivity of Ground-State Carbon Atoms with Unsaturated Hydrocarbons in Combustion Flames and in the Interstellar Medium. *Int. Rev. Phys. Chem.* **2002**, *21*, 307–356.
- (75) Miller, W. B.; Safron, S. A.; Herschbach, D. R. Exchange Reactions of Alkali Atoms with Alkali Halides. Collision Complex Mechanism. *Discuss. Faraday Soc.* **1967**, *44*, 108–122.
- (76) Shaik, S. S.; Canadell, E. Regioslectivity of Radical Attacks on Substituted Olefins. Application of the State-Correlation-Diagram (SCD) Model. *J. Am. Chem. Soc.* **1990**, *112*, 1446–1452.
- (77) Gannon, K. L.; Glowacki, D. R.; Blitz, M. A.; Hughes, K. J.; Pilling, M. J.; Seakins, P. W. H. Atom Yields from the Reactions of CN Radicals with C_2H_2 , C_2H_4 , C_3H_6 , Trans-2- C_4H_8 , and iso- C_4H_8 . *J. Phys. Chem. A* **2007**, *111*, 6679–6692.
- (78) Kaiser, R. I.; Stranges, D.; Bevsek, H. M.; Lee, Y. T.; Suits, A. G. Crossed-Beam Reaction of Carbon Atoms with Hydrocarbon Molecules. IV. Chemical Dynamics of Methylpropargyl Radical Formation, C_4H_5 , from Reaction of C (${}^3\text{P}_J$) with Propylene, C_3H_6 ($\text{X}_{1\text{A}}$). *J. Chem. Phys.* **1997**, *106*, 4945–4953.
- (79) Kaiser, R. I.; Ting, J. W.; Huang, L. C. L.; Balucani, N.; Asvany, O.; Lee, Y. T.; Chan, H.; Stranges, D.; Gee, D. A Versatile Source to Produce High-Intensity, Pulsed Supersonic Radical Beams for Crossed-Beam Experiments: The Cyanogen Radical CN ($\text{X}^2 \Sigma^+$) as a Case Study. *Rev. Sci. Instrum.* **1999**, *70*, 4185–4191.